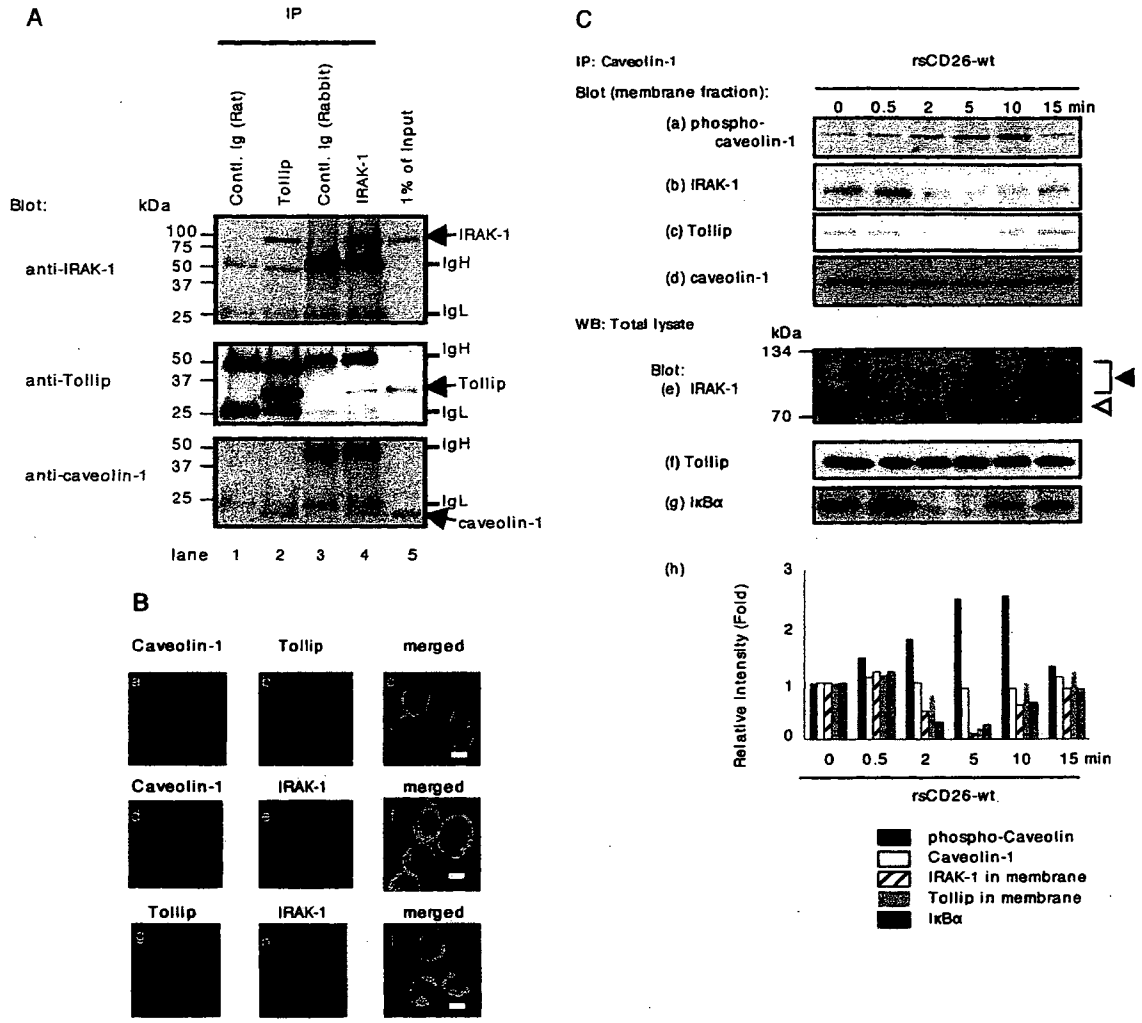

FIG. 2. Caveolin-1 complexes with Tollip and IRAK-1 in monocytes. A. After being pulsed with TT, freshly isolated monocytes were lysed, and IP assays were conducted with anti-Tollip, anti-IRAK-1 antibodies, or control Ig. IP complexes were then separated using 5 to 20% SDS-PAGE followed by Western blotting and were immunoblotted with the indicated antibodies. Shown are the representative results obtained in five independent experiments. IgH and IgL denote immunoglobulin heavy chain and immunoglobulin light chain, respectively. B. TT-loaded monocytes were attached to poly-L-lysine-coated coverslips, fixed with paraformaldehyde, and permeabilized using 0.05% Triton X-PBS. Cells were then stained with anti-caveolin PAb (a and d), anti-Tollip MAb (b and g), or anti-IRAK-1 PAb (e and h), followed by staining with fluorescein isothiocyanate- or Texas red-conjugated secondary antibodies. Cells were visualized by confocal laser microscopy. Observations were made on 50 cells in each of five independent experiments. The micrographs are representative of more than 75% of the cells observed. Bars indicate a 10-μm scale. C. TT-loaded monocytes were stimulated with rsCD26-wt-coated beads for the indicated time periods. Membrane proteins were extracted and immunoprecipitated with anti-caveolin-1 antibody, and immune complexes were resolved by 5 to 20% SDS-PAGE and immunoblotted with anti-phospho-caveolin-1 (a), anti-IRAK-1 (b), or anti-Tollip (c) antibodies, followed by stripping and reprobing with anti-caveolin-1 antibody (d). Total cell lysates from monocytes stimulated as described above were also resolved by 5 to 20% SDS-PAGE and immunoblotted with anti-IRAK (e), anti-Tollip (f), or anti-IκBα (g) antibodies. Position of IRAK-1 bands in e was indicated by an open triangle, and supershifted bands of IRAK-1 were indicated by a solid triangle. The reciprocal intensities of phospho-caveolin-1, caveolin-1, Tollip, and IRAK-1 in membrane proteins that were immunoprecipitated by anti-caveolin-1 were demonstrated (h). The reciprocal intensity of IκBα in total cell lysates was also demonstrated (h). Similar results were obtained in five independent experiments. WB, Western blot.

tagged Tollip mutants were cotransfected into COS cells with HA-tagged caveolin-1–wt (Cav-wt) and VSV-tagged IRAK-1–wt and then precipitated with anti-FLAG MAb. As shown in Fig. 3D, Cav-wt and IRAK-1–wt were coprecipitated with Tollip-wt and Tollip-C2+CUE (lanes 2 and 3). On the other hand, Tollip-ΔCUE and Tollip-C2 coprecipitated only with Cav-wt but not with IRAK-1–wt (lanes 4 and 6), while Tollip-ΔC2 coprecipitated with IRAK-1–wt but not with Cav-wt (lane 5). These data implied that the Tollip C2 domain was required for binding to caveolin-1 and that, as described previously (5), the Tollip CUE domain was required for binding to IRAK-1. Moreover, our findings strongly suggest that caveolin-1 is associated with IRAK-1 and Tollip containing both the C2 and CUE domains. To examine whether caveolin-1 was directly bound to IRAK-1, we next performed IP study with series of HA-tagged caveolin-1 mutants which were cotransfected into COS cells with FLAG-tagged Tollip-wt or Tollip-ΔC2 and VSV-tagged IRAK-1–wt or IRAK-1–ΔCT. As shown in Fig.

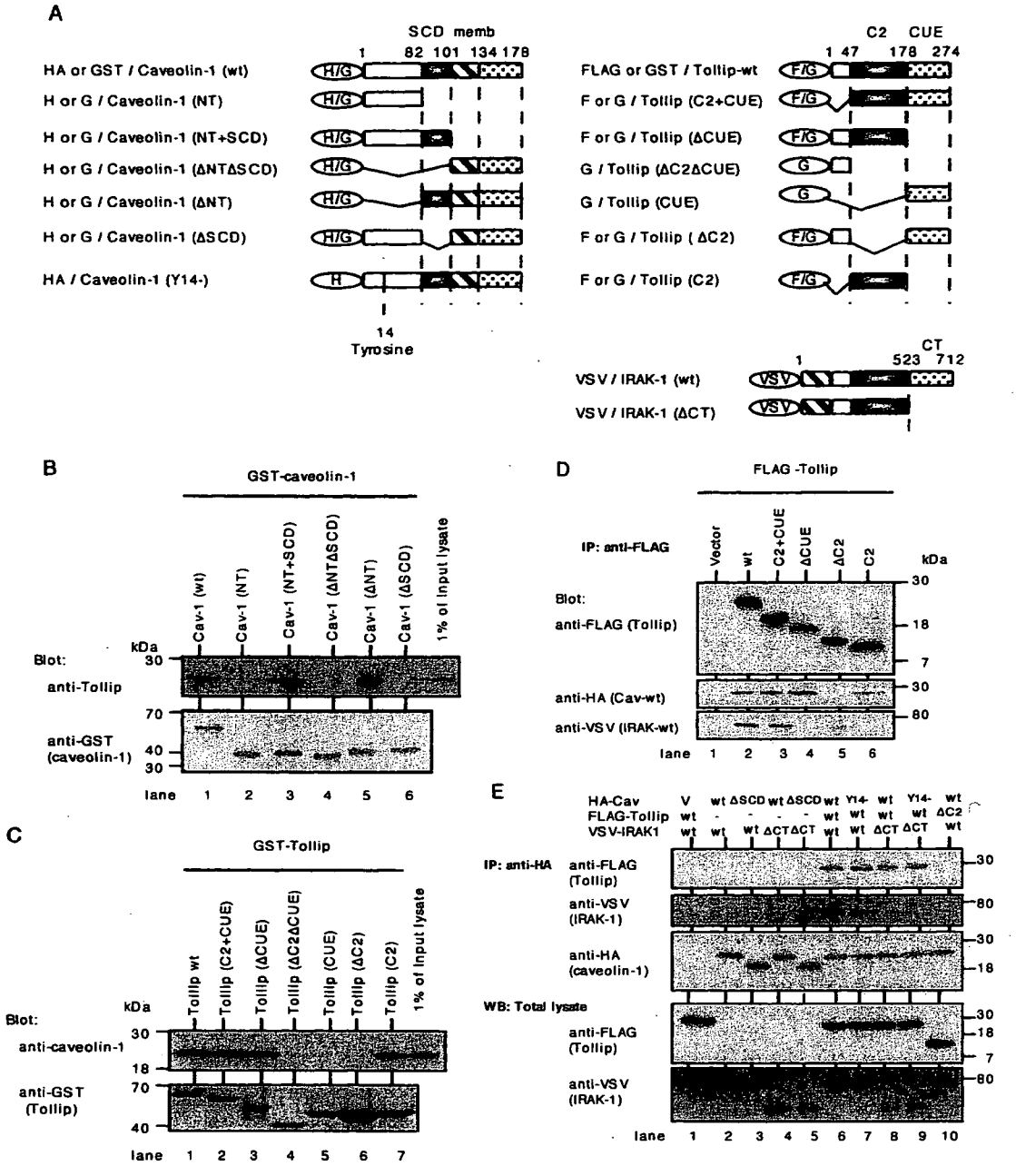

FIG. 3. Determination of the binding domains involved in the interaction among caveolin-1, Tollip, and IRAK-1. A. Schematic representation of HA-tagged or GST-fused caveolin-1, FLAG-tagged or GST-fused Tollip, VSV-tagged IRAK-1, and their mutants. In caveolin-1, residues 1 to 81 comprised the N-terminal region (NT) (open square), residues 82 to 101 comprised the scaffolding domain (SCD) (black square), residues 102 to 134 comprised the transmembrane region (memb; striped square), and residues 135 to 178 comprised the C-terminal region (dotted square). In Tollip, residues 47 to 178 comprised the protein kinase C conserved region 2 (C2 domain) (black square), and residues 179 to 274 comprised coupling of ubiquitin conjugation to endoplasmic reticulum degradation domain (CUE) (dotted square). In IRAK-1, residues 523 to 712 comprised the C-terminal domain (CT) (dotted square). H, G, and F denote HA, GST, and FLAG, respectively. B. GST-fused caveolin-1 and deletion mutants on glutathione-Sepharose (GSH) beads were incubated with THP-1 cell lysate after preclearing with GST on GSH beads. Bound proteins and a 1% amount of input lysate were resolved by 5 to 20% SDS-PAGE and immunoblotted with anti-Tollip MAb, followed by stripping and reprobing with anti-GST MAb. Similar results were obtained in three independent experiments. C. GST-fused Tollip and deletion mutants on GSH beads were incubated with THP-1 cell lysate after preclearing with GST on GSH beads. Bound proteins and a 1% amount of input lysate were resolved by 5 to 20% SDS-PAGE and immunoblotted with anti-caveolin-1 PAb, followed by stripping and reprobing with anti-GST MAb. Similar results were obtained in three independent experiments. D. COS cells were transfected with FLAG-tagged Tollip mutants, HA-tagged caveolin-1–wt, and VSV-tagged IRAK-1–wt, lysed, and immunoprecipitated with anti-FLAG (M2) MAb. Elutions of the FLAG-fusion protein complex were conducted by adding 150 ng/ml of 3× FLAG peptide. The eluted samples were separated using 5 to 20% SDS-PAGE and immunoblotted with anti-HA (caveolin-1–wt) or anti-VSV (IRAK-1–wt) PAbs, followed by stripping and reprobing with anti-FLAG (M2) MAb. Similar results were obtained in three independent experiments. E. COS cells were transfected with HA-tagged caveolin-1, FLAG-tagged Tollip, VSV-tagged IRAK-1, and mutants, lysed, and immunoprecipitated with agarose-conjugated anti-HA MAb. IPs were separated using 5 to 20% SDS-PAGE and immunoblotted with anti-FLAG (M2) (Tollip) MAb or anti-VSV (IRAK-1) PAb, followed by stripping and reprobing with anti-HA (caveolin-1) MAb (top three panels). Whole lysates of COS cells transfected as described above were separated using 5 to 20% SDS-PAGE to resolve expression of transfected FLAG-tagged Tollip and VSV-tagged IRAK-1 and mutants (bottom two panels). Similar results were obtained in three independent experiments. WB, Western blot.

3E, Tollip-wt and IRAK-1–wt were coprecipitated with caveolin-1 (lane 6). On the other hand, IRAK-1 was not coprecipitated with caveolin-1 in the absence of Tollip (lanes 2 to 5), and Cav-wt did not coprecipitate with IRAK-ΔCT even in the presence of Tollip-wt (lane 8). Moreover, Cav-wt did not coprecipitate with Tollip-ΔC2 and IRAK-1-wt (lane 10). Taken together, the above-described results support the notion that the SCD of caveolin-1 binds to the C2 domain of Tollip, the CUE domain of which binds to the C-terminal (CT) domain of IRAK-1. It was observed that caveolin-1 does not bind to IRAK-1 directly.

In the previous study, we showed that caveolin-1 was phosphorylated by CD26 stimulation and transduced signaling events to upregulate CD86 (43). To examine whether phosphorylation of caveolin-1 affected binding to Tollip and IRAK-1, we constructed deletion mutant of tyrosine at residue 14 of caveolin-1 (HA-Cav-Y14)$^-$, and IP study was conducted as described above. As shown in Fig. 3E, the binding capacity of this tyrosine-deleted caveolin-1 to Tollip (lanes 7 and 9) and IRAK-1 (lane 7) did not change compared to that of Cav-wt (lanes 6 and 8). On the other hand, rsCD26-wt was coprecipitated with HA-Cav-Y14, which was not observed to be phosphorylated, while HA-Cav-wt transfected into HEK293 cells was phosphorylated by exogenous rsCD26-wt (data not shown). These results suggest that Cav-Y14 does not affect binding to Tollip and IRAK-1.

Subcellular colocalization of caveolin-1, Tollip, and IRAK-1 in living cells. To confirm the above-described findings in living cells, we performed immunocytochemical analysis with HEK293 cells which were cotransfected with series of caveolin-1, Tollip, and IRAK-1 mutants. GFP-fused or HA-tagged caveolin-1–wt was cotransfected with FLAG-tagged Tollip-wt or Tollip-ΔC2 and VSV-tagged IRAK-1–wt or IRAK-1–ΔCT and stained with anti-FLAG MAb or anti-VSV PAb. As shown in Fig. 4a to c, wild-type proteins of caveolin-1, Tollip, and IRAK-1 were colocalized with each other. On the other hand, caveolin-1–GFP was not colocalized with Tollip-ΔC2 (Fig. 4d) or with IRAK-1–wt in the presence of Tollip-ΔC2 (Fig. 4e), while Tollip-ΔC2 was colocalized with IRAK-1–wt (Fig. 4f). Moreover, following transfection with IRAK-1–ΔCT, caveolin-1–GFP and Tollip-wt were colocalized (Fig. 4g), while IRAK-1–ΔCT was not colocalized with caveolin-1–GFP or with Tollip-wt (Fig. 4h and i). Furthermore, following transfection with Tollip-ΔCUE, caveolin-1–GFP and Tollip-ΔCUE were colocalized, but IRAK-1–wt was not colocalized with caveolin-1–GFP or with Tollip-ΔCUE (data not shown). These data strongly suggest that the SCD of caveolin-1 binds to the C2 domain of Tollip and that the CUE domain of Tollip binds to the CT domain of IRAK-1.

Tollip and IRAK-1 are necessary to enhance human CD86 promoter activity via CD26–caveolin-1 interaction through tyrosine phosphorylation at residue 14 of caveolin-1. In the previous report, we revealed that NF-κB activation downstream of cavelin-1 resulted in the upregulation of CD86 in TT-loaded monocytes stimulated with exogenous CD26 (43). From our present results, we hypothesized that Tollip and IRAK play a role in CD86 upregulation in monocytes downstream of the interaction between CD26 and caveolin-1. To confirm this hypothesis, we evaluated CD86 promoter activity following the interaction between CD26 and caveolin-1 in the presence or absence of Tollip and IRAK-1 by using luciferase chimera of the 5′-flanking promoter region of human CD86 (a 1.3-kb fragment upstream of the transcriptional site of the CD86 gene), which was described previously (43). CD86 promoter activity was enhanced following cotransfection of Tollip-wt in a dose-dependent manner in the presence of caveolin-1–wt (Fig. 5A, top). However, CD86 promoter activity was not detected in the presence of Tollip-ΔC2 or Tollip-ΔCUE with caveolin-1–wt or caveolin-1 Y14 (Fig. 5A, top). Moreover, increasing doses of IRAK-1–wt resulted in increased activity of the CD86 promoter with caveolin-1–wt but not with caveolin-1 Y14 (Fig. 5B, top). Moreover, CD86 promoter activity was not detected in the presence of IRAK-ΔCT with caveolin-1–wt or caveolin-1 Y14 (Fig. 5B, top). On the other hand, activation of the CD86 promoter was not observed by stimulation with CD26 lacking the CBD (CD26-Δ201) or with medium alone (middle and bottom panels of Fig. 5A and

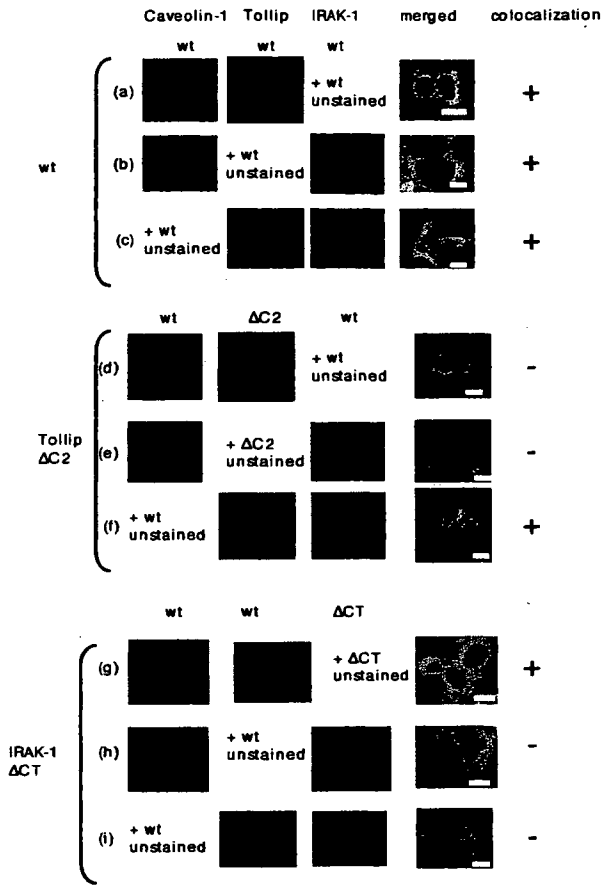

FIG. 4. Subcellular colocalization of caveolin-1, Tollip, and IRAK-1 in living cells. HEK293FT cells were transfected with GFP-fused (a, b, d, e, g, and h) or HA-tagged (c, f, and i) caveolin-1-wt, FLAG-tagged Tollip (wt or ΔC2), and VSV-tagged IRAK-1 (wt or ΔCT). Cells were then fixed and permeabilized with acetone-methanol and stained with anti-FLAG (M2) MAb or anti-VSV PAb, followed by staining with anti-mouse Ig (fluorescein isothiocyanate- or Texas red-conjugated) or anti-rabbit Ig (Texas red-conjugated) antibodies. Stained cells were mounted using a Prolong Antifade kit. Observations were made with 10 to 15 cells in each of five different experiments. The micrographs are representative of more than 75% of the cells observed. Bars indicate a 10-μm scale.

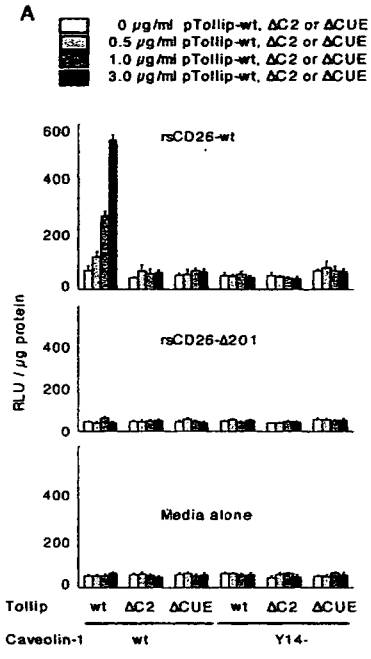

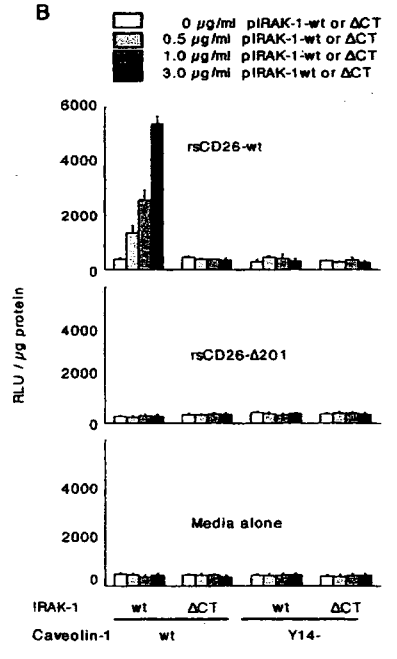

FIG. 5. Enhanced CD86 promoter activity by increasing doses of Tollip or IRAK-1 in response to exogenous CD26 stimulation. A. Twelve hours after HEK293 cells were cotransfected with human CD86-promoter luciferase constructs, caveolin-1 (wt or deleting tyrosine at residue 14 mutant [Y14⁻]) and Tollip (wt, ΔC2, or ΔCUE) vectors, wild-type-soluble CD26 (rsCD26-wt), or rsCD26 lacking the caveolin-binding domain (rsCD26-Δ201) was added to the culture medium and incubated for an additional 20 h. Cells were harvested for measurement of luciferase activity and protein concentration. Luciferase activity is shown as being relative to 1 μg of applied protein. Data represent means ± standard errors (SE) from triplicate experiments. B. HEK293 cells were cotransfected with human CD86-promoter luciferase constructs, caveolin-1 (wt or Y14⁻), and IRAK-1 (wt or ΔCT) vectors, treated, and prepared for luciferase assay as described above. RLU, relative light units.

B). These data strongly suggest that tyrosine phosphorylation of caveolin-1 at residue 14 is necessary to induce activation of NF-κB to upregulate CD86 expression via Tollip and IRAK-1 following CD26–caveolin-1 interaction.

siRNA against Tollip attenuates CD26-mediated upregulation of CD86 and inhibits T-cell proliferation driven by tetanus toxoid. To examine CD26–caveolin-1–Tollip interaction on TT-mediated T-cell proliferation more directly, we performed siRNA experiments in freshly isolated monocytes. For this purpose, we prepared two sets of specific siRNAs against Tollip as described in Materials and Methods, and both of these siRNAs decreased Tollip expression in monocytes (Fig. 6A, lanes 3 and 4). Since Tollip expression in monocytes was not significantly affected by HVJ-E vector or mismatched siRNA (lanes 2 and 5), this inhibitory effect by siRNA was specific. siRNA or HVJ-E vector did not affect expression levels of IRAK-1 and caveolin-1 (Fig. 6A). We next examined whether exogenously added CD26 exerted its effect on monocytes in which Tollip expression was attenuated by siRNA. For this purpose, freshly isolated monocytes that were untreated or treated with siRNA against Tollip were incubated with rsCD26-wt or CD26-Δ201 beads in the presence or absence of TT, and the expression of CD86 on monocytes was examined using flow cytometric analysis. As shown in Fig. 6B, CD86 expression on monocytes with medium alone or mis-siRNA treatment was increased significantly after TT and rsCD26-wt stimulation (Fig. 6B) as reported previously (42, 43). This enhancing effect was not observed following treatment with rsCD26-Δ201 beads, which did not stimulate caveolin-1 on monocytes (Fig. 6B). On the other hand, treatment with siRNA against Tollip in monocytes resulted in a significant decrease in CD86 expression when monocytes were pulsed with TT and rsCD26-wt beads (Fig. 6B). In fact, the CD86 expression level in these monocytes (Fig. 6B) was similar to the level seen in monocytes that were not treated other than with TT plus rsCD26-wt (Fig. 6B). These results suggest that Tollip plays an important role in signal transduction following CD26 binding to TT-loaded monocytes, leading to the upregulation of CD86, as shown in our previous study using monocytes of caveolin-1 knockdown (43).

In the previous study, we demonstrated that activation of NF-κB was involved in upregulation of CD86 following CD26–caveolin-1 interaction (43). In Fig. 1 and 2, we showed that Tollip mediates activation of NF-κB via phosphorylation of caveolin-1 by exogenous CD26. To elucidate the more direct effect of Tollip on inducing activation of NF-κB, we examined activation of NF-κB using an ELISA-based DNA-binding detection method. As shown in Fig. 6C, We detected significant levels of the p50 and p65 NF-κB components in nuclear extracts (NE) of TT-loaded monocytes stimulated with wild-type CD26 (Fig. 6C). The increase in p50 and p65 NF-κB levels was inhibited by treatment of siRNA against Tollip (Fig. 6C). On

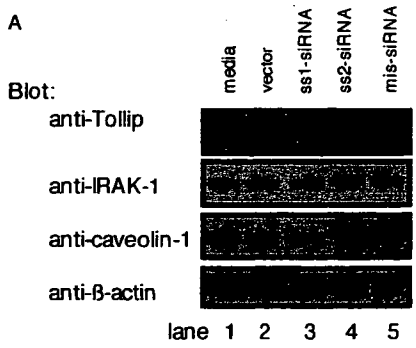
A
media
vector
ss1-siRNA
ss2-siRNA
mis-siRNA
Blot:
anti-Tollip
anti-IRAK-1
anti-caveolin-1
anti-ß-actin
lane 1 2 3 4 5

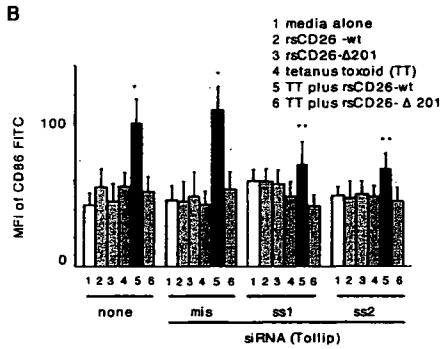
B
1 media alone
2 rsCD26 -wt
3 rsCD26-Δ201
4 tetanus toxoid (TT)
5 TT plus rsCD26-wt
6 TT plus rsCD26- Δ 201
MFI of CD86 FITC
100
0
1 2 3 4 5 6
none
mis
ss1
ss2
siRNA (Tollip)

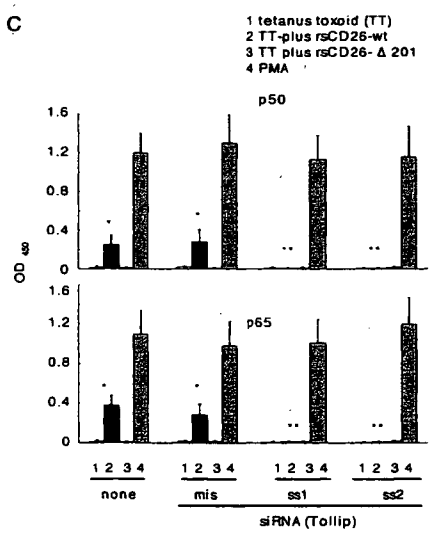
C
1 tetanus toxoid (TT)
2 TT-plus rsCD26-wt
3 TT plus rsCD26- Δ 201
4 PMA
p50
p65
OD 450
1.6
1.2
0.8
0.4
0
1 2 3 4
none
mis
ss1
ss2
siRNA (Tollip)

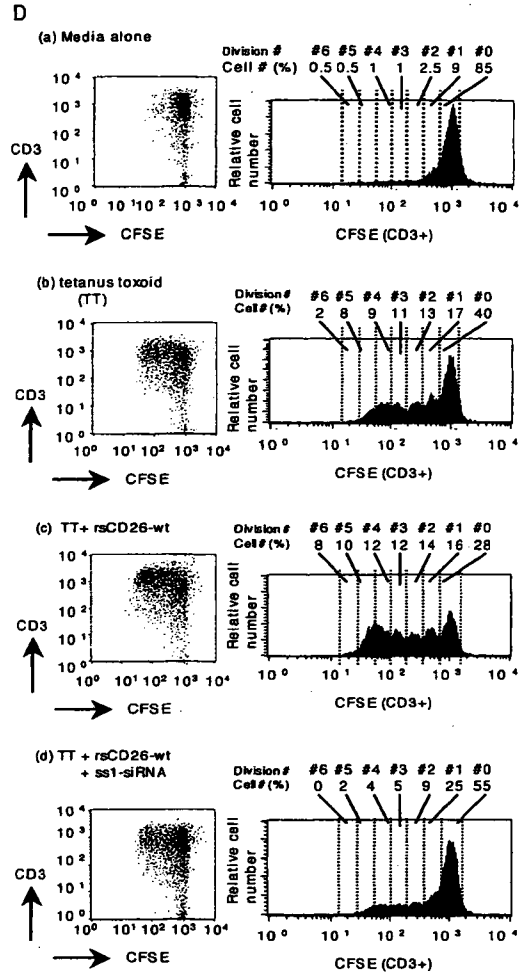
D
(a) Media alone
Division #
Cell # (%)
#6 #5 #4 #3 #2 #1 #0
0.5 0.5 1 1 2.5 9 85
CD3
CFSE
Relative cell number
CFSE (CD3+)
(b) tetanus toxoid (TT)
2 8 9 11 13 17 40
(c) TT+ rsCD26-wt
8 10 12 12 14 16 28
(d) TT + rsCD26-wt + ss1-siRNA
0 2 4 5 9 25 55

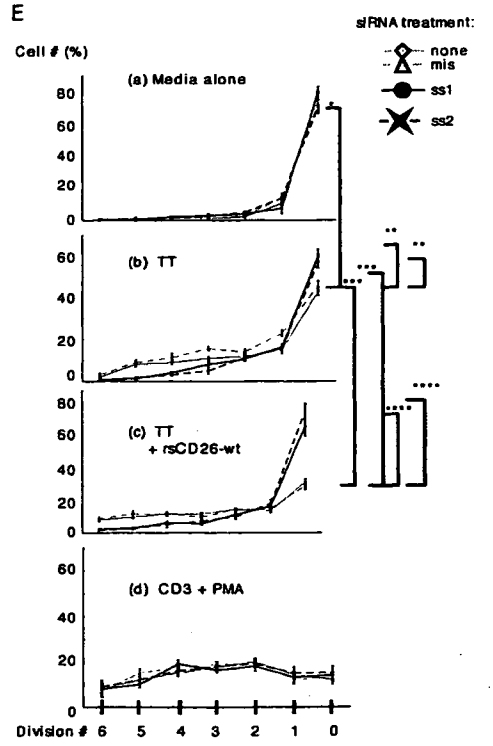
E
siRNA treatment:
none
mis
ss1
ss2
Cell # (%)
(a) Media alone
(b) TT
(c) TT
+ rsCD26-wt
(d) CD3 + PMA
Division # 6 5 4 3 2 1 0

the other hand, the levels of p50 and p65 NF-κB did not alter in NE of TT-loaded monocytes stimulated with TT alone or with CD26 lacking the CBD (CD26-Δ201) (Fig. 6C), and siRNA treatment did not alter activation of p50 and p65 by PMA (Fig. 6C). These results strongly suggest that Tollip plays an important role in signal transduction to activate of NF-κB following CD26 binding to TT-loaded monocytes, leading to the upregulation of CD86, as shown in our previous study using caveolin-1 knockdown monocytes (43).

Furthermore, to determine whether T-cell proliferation pulsed with TT was inhibited in the presence of monocytes with decreased Tollip expression, proliferation assays were performed using CFSE as described in Materials and Methods, with purified T cells being from the same donor as the prepared monocytes. In studies involving the CFSE fluorescent profile, TT-induced T-cell proliferation was observed in the presence of monocytes with unaffected Tollip levels (Fig. 6D, panels a and b), as demonstrated by the increased numbers of CFSE fluorescence intensity of $CD3^+$ cells. Meanwhile, TT-induced T-cell proliferation was significantly enhanced in the presence of exogenous rsCD26 (Fig. 6D, panel c), as described previously (42, 43, 57). This effect was clearly inhibited by Tollip knockdown (Fig. 6D, panel d). To quantify these observations, cell numbers to each cell division number determined by CFSE fluorescence intensity of $CD3^+$ subset with or without various treatments were demonstrated in line graphs (Fig. 6E). TT-induced T-cell proliferation was observed without Tollip knockdown (Fig. 6E), and this proliferation was significantly inhibited by Tollip knockdown in monocytes (Fig. 6E). On the other hand, as described previously (42, 43, 57), TT-induced T-cell proliferation was significantly enhanced in the presence of exogenous rsCD26 (Fig. 6E). This effect was more profoundly suppressed by Tollip knockdown than the inhibition observed with TT alone (Fig. 6E). Knockdown of Tollip in monocytes did not have an effect on anti-CD3 plus PMA-stimulated T-cell proliferation (Fig. 6E, panel d). Moreover, rsCD26-Δ201 did not enhance TT-mediated T-cell proliferation (data not shown). These results demonstrate that Tollip has an important role in the enhancement of TT-induced T-cell proliferation following treatment with exogenous CD26.

siRNA against IRAK-1 attenuates CD26-mediated upregulation of CD86 and inhibits T-cell proliferation driven by tetanus toxoid. To examine directly the role of IRAK-1 in caveolin-1-induced CD86 activation, we performed siRNA experiments in freshly isolated monocytes. ss3-siRNA, designed for knockdown of human IRAK-1, decreased IRAK-1 expression in monocytes (Fig. 7A, lanes 3). We examined whether exogenously added CD26 exerted its effect on monocytes in which IRAK-1 expression was attenuated by ss3-siRNA. For this purpose, freshly isolated monocytes that were untreated or treated with siRNA against IRAK-1 were incubated with rsCD26-wt or rsCD26-Δ201 beads in the presence or absence of TT, and the expression of CD86 on monocytes was examined using flow cytometric analysis. As shown in Fig. 7B, CD86 expression on monocytes treated with medium alone or mis-siRNA was increased significantly after TT and rsCD26-wt stimulation, as reported previously (42, 43) and as observed in Fig. 6B. This enhancing effect was not observed following treatment with rsCD26-Δ201 beads, which did not stimulate caveolin-1 on monocytes (Fig. 7B). On the other hand, treatment with siRNA against IRAK-1 in monocytes resulted in a significant decrease in CD86 expression when monocytes were pulsed with TT and rsCD26-wt beads (Fig. 7B). In fact, the CD86 expression level in these monocytes (Fig. 7B) was similar to the level seen in monocytes treated with stimuli other than rsCD26-wt plus TT (Fig. 7B). These results suggest that IRAK-1 also plays an important role in signal transduction following CD26 binding to TT-loaded monocytes, leading to the upregulation of CD86, as shown in our previous study using Tollip (Fig. 6B) or caveolin-1 knockdown monocytes (43).

Moreover, we detected significant levels of the p50 and p65

FIG. 6. siRNAs against Tollip inhibit the effect of exogenous CD26 on CD86 upregulation in TT-loaded monocytes and proliferation of T cells in response to TT. A. Purified monocytes were transfected with or without sense siRNA (ss1 is targeted for positions +186 to +206, and ss2 is targeted for positions +774 to +794) of the Tollip gene or mismatched siRNA (mis-siRNA) by using the HVJ-E vector. Cell lysates were resolved by 5 to 20% SDS-PAGE and immunoblotted with the indicated antibodies, followed by stripping and reprobing with anti-β-actin antibody. All experiments were performed at least five times with similar results. B. Purified monocytes were transfected with or without siRNA using the HVJ-E vector, followed by treatment with TT. After stimulation with rsCD26 (wt or Δ201)-coated beads, cells were subjected to analysis of surface CD86 expression by flow cytometry. Monocytes were identified by gating of the CD45-Cy Chrome- and CD14-phycoerythrin-positive population. Mean fluorescence intensity (MFI) of cell surface CD86 is demonstrated. Data represent means ± SE of five independent experiments. * shows points of significant increase ($P < 0.05$), whereas ** indicates points of no significant change compared to controls. FITC, fluorescein isothiocyanate. C. TT-loaded monocytes with or without siRNA treatment were stimulated with CD26-coated beads and harvested for extraction of nuclear proteins (NE). Each 5 μg of NE was subjected to an ELISA-based DNA-binding protein assay. Binding activity to p50 and p65 NF-κB components was revealed by an optical density value at 450 nm (OD_{450}). Data represent means ± SE from triplicate experiments. * shows points of significant increase ($P < 0.05$), whereas ** indicates points of no significant change compared to controls. D. Kinetic analyses of T-cell division as proliferation in populations of CFSE-labeled T cells. Isolated T cells were labeled with CFSE and cultured for 96 h with monocytes isolated from the same donor. T cells were cocultured with untreated monocytes (a), with TT-loaded monocytes (b), with TT-loaded monocytes followed by addition of rsCD26-wt (c), and with siRNA ss1-treated monocytes pulsed with TT and rsCD26-wt (d). T cells were revealed by $CD3^+$ populations in dot plots as shown in the left panels. Histograms of the right panels show the CFSE fluorescence profile of $CD3^+$ subsets from each dot gram. The numbers appearing above each histogram denote each division population (upper "Division #") and percent cell numbers in each division [lower "Cell # (%)"]. The undivided T cells reside in the rightmost peak, and the T cells having divided six times reside in the leftmost peak. The experiment depicted here is representative of five separate experiments. E. Kinetic analyses of T-cell division as proliferation in populations of CFSE-labeled T cells were shown as sequential line graphs, conducted as described above (C). T cells were cocultured with untreated monocytes (a), with TT-loaded monocytes (b), with TT-loaded monocytes followed by addition of rsCD26-wt (c), and in the presence of soluble anti-CD3 plus PMA (d). Before coculture with T cells, monocytes were treated with or without siRNAs as described in Materials and Methods. The numbers appearing under each graph denote each division population (Division #), and the verticals are the percent cell numbers in each division [Cell # (%)]. Data represent means ± SE from triplicate experiments. Asterisks depict significant changes ($P < 0.05$).

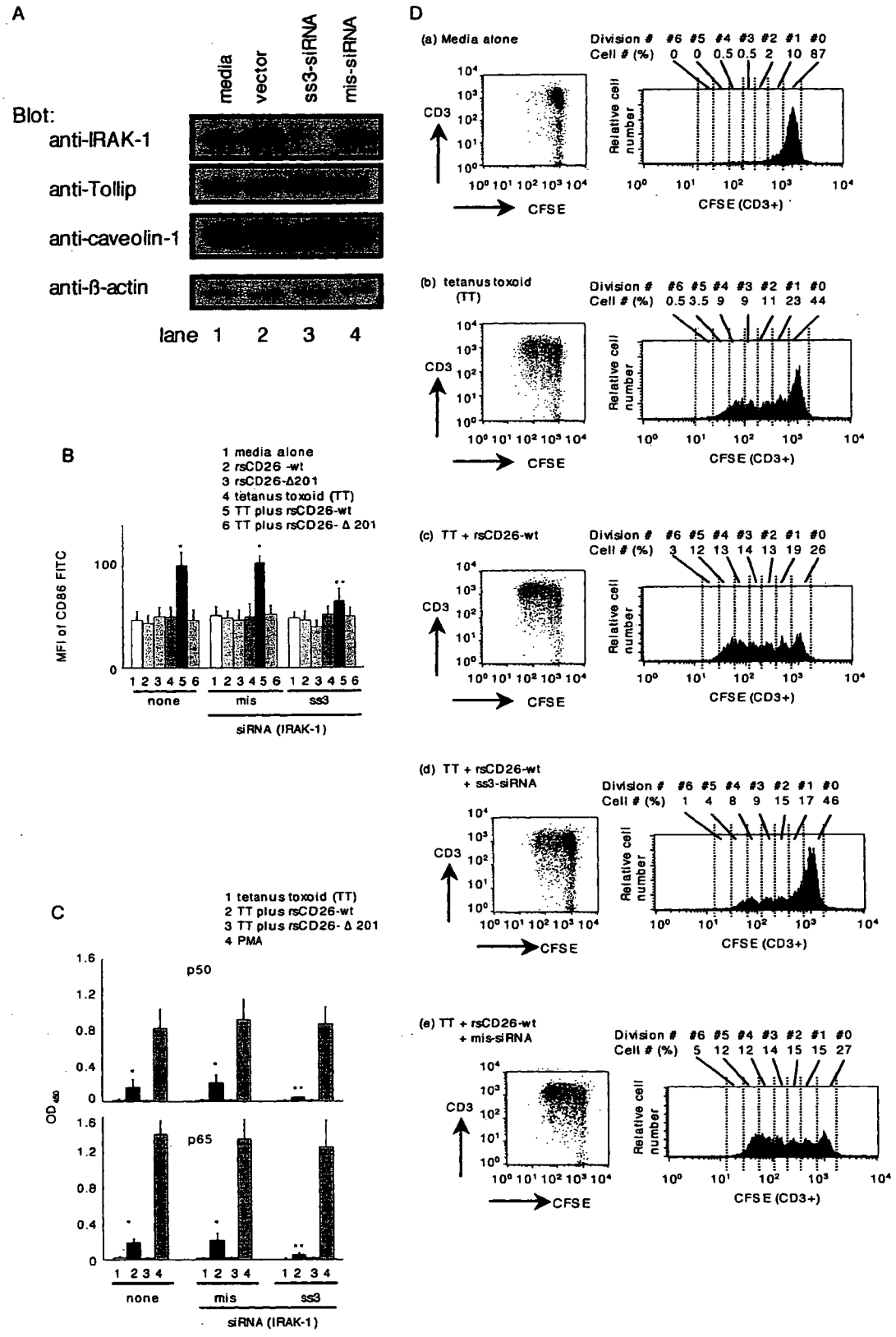

FIG. 7. siRNAs against IRAK-1 inhibit the effect of exogenous CD26 on CD86 upregulation in TT-loaded monocytes and proliferation of T cells in response to TT. A. Purified monocytes were transfected with or without ss3-siRNA (targeted for positions +969 to +989 of human IRAK-1 gene) or mismatched siRNA (mis-siRNA) by using the HVJ-E vector. Cell lysates were resolved by 5 to 20% SDS-PAGE and immunoblotted with the indicated antibodies, followed by stripping and reprobing with anti-β-actin antibody. All experiments were performed at least five times with

NF-κB components in NE of TT-loaded monocytes stimulated with wild-type CD26 (Fig. 7C), and the increase in p50 and p65 NF-κB levels was inhibited by treatment of siRNA against IRAK-1 (Fig. 7C). On the other hand, the levels of p50 and p65 NF-κB did not alter in NE of TT-loaded monocytes stimulated with TT alone or with CD26 lacking the CBD (CD26-Δ201), and siRNA treatment did not affect activation of p50 or p65 by PMA (Fig. 7C). These results strongly suggest that IRAK-1 also plays an important role in signal transduction to activate NF-κB following CD26 binding to TT-loaded monocytes, leading to the upregulation of CD86, as shown in Fig. 6 using siRNA against Tollip and as observed in our previous study using caveolin-1 knockdown monocytes (43).

Finally, to determine whether T-cell proliferation pulsed with TT was inhibited in the presence of monocytes with decreased IRAK-1 expression, proliferation assays were performed using CFSE, similar to the methods used for the studies described in the legend of Fig. 6D and E. In studies involving the CFSE fluorescent profile, TT-induced T-cell proliferation was observed in the presence of monocytes with unaffected IRAK-1 levels (Fig. 7D, panels a and b). Despite the fact that TT-induced T-cell proliferation was significantly enhanced in the presence of exogenous rsCD26 (Fig. 7D, panel c), this effect was clearly inhibited by IRAK-1 knockdown (Fig. 7D, panel d). Mismatched siRNA (mis-siRNA) did not alter enhancement of exogenous CD26-mediated T-cell proliferation, and knockdown of IRAK-1 in monocytes did not have an effect on anti-CD3 plus PMA-stimulated T-cell proliferation (data not shown). These results demonstrate that IRAK-1 has an important role in the enhancement of TT-induced T-cell proliferation following treatment with exogenous CD26.

DISCUSSION

In the previous study, we identified caveolin-1 in APC as a binding protein for CD26 and demonstrated that external CD26 stimulation induced phosphorylation of caveolin-1 to enhance surface expression of CD86 on APC by activation of NF-κB (43). This interaction resulted in enhancing CD26-mediated T-cell proliferation in response to recall antigen such as TT (42, 43). However, it remains to be elucidated as to how caveolin-1 is linked to the activation of NF-κB in monocytes.

In the present study, we demonstrated that caveolin-1 binds to Tollip and IRAK-1 in the membrane of TT-loaded monocytes and that following exogenous CD26 stimulation, Tollip and IRAK-1 disengage from caveolin-1, with IRAK-1 being subsequently phosphorylated to upregulate CD86 expression. Moreover, we showed that Tollip plays an important role in the interaction among caveolin-1, Tollip, and IRAK-1 and in CD26–caveolin-1 signaling to upregulate CD86, resulting in subsequent T-cell proliferation in response to TT.

To identify the proteins associated with caveolin-1 following exogenous CD26 stimulation, we conducted proteomic analysis of TT-loaded monocytes in the presence or absence of exogenous CD26 stimulation and identified a decrease in the level of Tollip and IRAK-1 among membrane proteins following CD26-wt stimulation (Fig. 1). It was previously reported that Tollip was involved in IL-1R/Toll-like receptor (TLR)-mediated signaling and that it linked IRAK to NF-κB, Jun N-terminal protein kinase, and p38 mitogen-activated protein kinase (7, 10). Originally, Tollip was cloned as a protein that interacts with the IL-1R accessory protein (5). Subsequently, Tollip was shown to associate directly with the cytoplasmic TIR domains of IL-1Rs, TLR2, and TLR4 following the stimulation of these receptors and to inhibit TLR-mediated cellular responses by suppressing the phosphorylation and kinase activity of IRAK-1 (62). In resting cells, Tollip forms a complex with members of the IRAK family, thereby preventing NF-κB activation by blocking the phosphorylation of IRAK-1. After receptor activation, Tollip–IRAK-1 complexes are recruited to the IL-1Rs TLR2 and TLR4, which results in the rapid autophosphorylation of IRAK-1 and its dissociation from the receptors. At the same time, IRAK-1 phosphorylates Tollip, which might then lead to the dissociation of Tollip from IRAK-1 and to its rapid ubiquitylation and degradation (25, 50). Tollip is therefore thought to function mainly to maintain immune cells in a quiescent state and to facilitate the termination of IL-1R/TLR-induced cell signaling during inflammation and infection. However, our present findings showed that Tollip in TT-loaded monocytes functioned as a recruiter of IRAK-1 to caveolin-1 after CD26-mediated phosphorylation of caveolin-1 and then transduced intracellular signals to activate NF-κB, leading to the upregulation of CD86 expression (Fig. 2C, 5A and B, and 6B to D). Moreover, other investigators reported that increased expression of Tollip was observed after LPS challenge, and thus, hyporesponsiveness to LPS was prolonged with Tollip serving as a suppressor (1, 30). However, we observed that the total expression level of Tollip did not change following exogenous CD26 stimulation and dissocia-

similar results. B. Purified monocytes were transfected with or without siRNA using the HVJ-E vector, followed by treatment with TT. After stimulation with rsCD26 (wt or Δ201)-coated beads, cells were subjected to analysis of surface CD86 expression by flow cytometry with the same method as described in the legend of Fig. 6B. Mean fluorescence intensity (MFI) of cell surface CD86 is demonstrated. Data represent means ± SE of five independent experiments. * shows points of significant increase ($P < 0.05$), whereas ** indicates points of no significant change compared to controls. FITC, fluorescein isothiocyanate. C. TT-loaded monocytes with or without siRNA treatment were stimulated with CD26-coated beads and harvested for extraction of nuclear proteins (NE). Each 5 μg of NE was subjected to an ELISA-based DNA-binding protein assay as described in the legend of Fig. 6C. Data represent means ± SE from triplicate experiments. * shows points of significant increase ($P < 0.05$), whereas ** indicates points of no significant change compared to controls. OD_{450}, optical density at 450 nm. D. Kinetic analyses of T-cell division as proliferation in populations of CFSE-labeled T cells using the same method as described in the legend of Fig. 6D. T cells were cocultured with untreated monocytes (a), with TT-loaded monocytes (b), with TT-loaded monocytes followed by addition of rsCD26-wt (c), and with ss3-siRNA-treated (d) or mis-siRNA-treated (e) monocytes pulsed with TT following rsCD26-wt stimulation. T cells were revealed by $CD3^+$ populations in dot plots as shown in the left panels. Histograms of the right panels show the CFSE fluorescence profile of $CD3^+$ subsets from each dot plot. The numbers appearing above each histogram denote each division population (upper "Division #") and percent cell numbers in each division [lower "Cell # (%)"]. The undivided T cells reside in the rightmost peak, and the T cells having divided six times reside in the leftmost peak. The experiment depicted here is representative of five separate experiments.

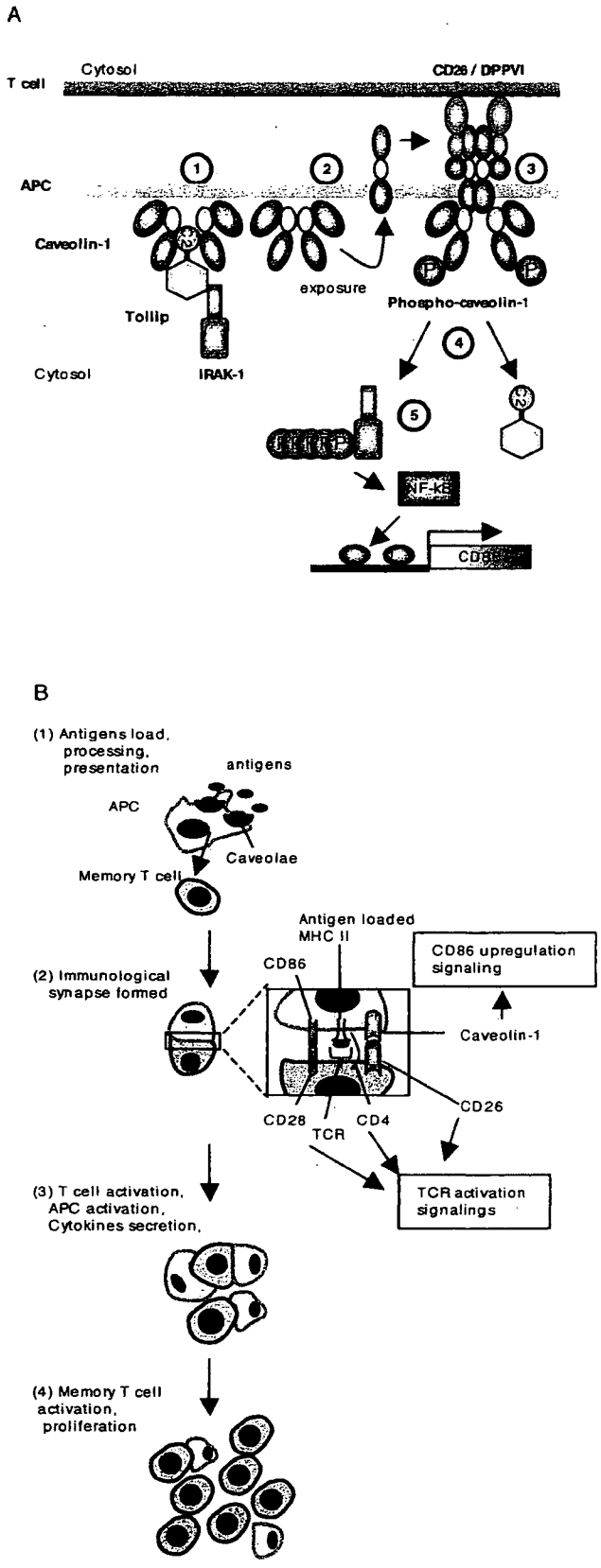

FIG. 8. Model for CD26–caveolin-1 interaction leading to upregulation of CD86. A. Caveolin-1 in monocytes (APC) resides at the inner membrane in the presence or absence of Tollip and IRAK-1 (1). After uptake of tetanus toxoid into monocytes via caveolae, some population of caveolin-1 is exposed on the outer cell surface of TT-loaded monocytes (2). Migration of $CD26^+$ antigen-specific memory T cells to areas of antigen-loaded APCs results in contact with TT APC, leading to the association of CD26 and caveolin-1 (3). Aggregation of caveolin-1 in the contact area occurs, presumably by homo-oligomerization (via its residues 61 to 101), followed by its phosphorylation. Phosphorylated caveolin-1 (phospho-caveolin-1) dissociates complexed Tollip and IRAK-1, presumably due to conformational changes, and IRAK-1 is then phosphorylated in the cytosol (4). After IRAK is phosphorylated, NF-κB is activated to lead to upregulation of CD86 (5). B. Antigens such as tetanus toxoid are loaded into monocytes and are then processed and presented with MHC class II (MHC II) on the cell surface along with exposure of caveolin-1 N terminus (1). Memory T cells expressing CD26 have contact with these antigen-presenting cells, and maturation of the immunological synapse occurs via T-cell receptor (TCR)-MHC class II, CD28-CD86/CD80, and CD26–caveolin-1 interactions (2). T cells and APC are then activated and cytokines are secreted (3). CD86 upregulation therefore leads to greater T-cell–APC interaction and the development of activated T cells locally and activated immune response, resulting in potential autoimmune diseases (4).

tion from caveolin-1, although the Tollip level in the cell membrane was decreased (Fig. 2C, panels c and f). Although the precise mechanism is not known, we speculate that a change in the total level of Tollip was not observed since only a small amount of membrane Tollip exists in comparison to excess level of Tollip in the cytoplasm (Fig. 2A and B). Although IRAK-M is a catalytically inactive kinase in monocytes that suppresses IRAK-1 function by inhibiting phosphorylation of IRAK-1 or preventing its dissociation from the receptor complex (26), we did not observe an association between caveolin-1 and IRAK-M (data not shown).

The generation of IRAK-1 knockout mice has revealed an important role for this kinase in signaling by TLR4 as well as the IL-1R (24, 53, 59). Cells lacking IRAK-1 exhibit an impaired ability to activate p38 mitogen-activated protein kinase, Jun N-terminal protein kinase, and NF-κB and to secrete inflammatory cytokines (e.g., tumor necrosis factor alpha [TNF-α] and IL-6) when stimulated with LPS or IL-1 (24, 53, 59). Notably, IRAK-1-deficient mice are less susceptible to the lethal effects of LPS than their wild-type counterparts (53). Despite this, whether IRAK-1 plays a role in immune response of memory T cells has not been described, presumably because there are many differences in adoptive immunity between mice and humans (36). In particular, $CD26^+$ T cells have different functions in mice and humans. In mice, the CD26 molecule was found as a thymocyte-activating molecule expressed on CD4 CD8 double-negative immature thymocytes, and this molecule might be involved in an important activation pathway during thymocyte differentiation (41). On the other hand, CD26 was originally characterized as a T-cell activation antigen in human T cells and expressed on $CD4^+$ or $CD8^+$ medullary thymocytes in the human thymus (39). Human CD26 is also preferentially expressed on a specific population of T lymphocytes, the subset of $CD4^+$ memory T cells, and is upregulated after T-cell activation (11, 12, 38). Thus, the murine system may not be appropriate for studying CD26 and adoptive immunity, especially compared to the human system.

Our findings, which establish a biochemical protein-protein association, raise questions about the functional implication of

caveolin-1 binding to Tollip and IRAK-1 as well as exogenous CD26. Many other receptor systems appear to localize to caveoli, which are defined by their cholesterol- and sphingomyelin-enriched lipid environments as well as by their morphological features (51). As an example, TNF receptor (TNFR)-associated factor 2 (TRAF2) is reported to be associated with caveolin-1 to activate NF-κB signaling by clustering caveolin-1–TRAF2 and TNFR2 (15). If exogenous CD26 were associated with caveolin-1 and TRAF2 clustering, 2D-PAGE analysis of membrane proteins of APC may detect changes in the levels of other proteins. However, we only observed changes in the levels of Tollip and IRAK-1, as shown in Fig. 1. Further study will be needed to determine whether caveolin-1–CD26 association alters signaling complexes other than Tollip and IRAK-1. Another issue raised by our findings is how the complex containing exogenous CD26 and caveolin-1 clusters with the complex containing Tollip and caveolin-1, since both CD26 and Tollip bind to the SCD of caveolin-1 (Fig. 3B and our previous report [43]). Our speculation is as follows: a part of caveolin-1 binds to Tollip in the cytoplasm, while another part of caveolin-1 binds to exogenous CD26 following the external exposure of caveolin-1 that accompanies processing of TT. Both heterocomplexes may associate with each other via interaction of the homo-oligomerization domain (residues 61 to 101) of caveolin-1 (49, 52). It would be of considerable interest to define this interaction in future studies. Degradation of IRAK-1 after CD26–caveolin-1 stimulation is another issue to be elucidated. It has been reported that specific phosphorylated amino acids on IRAK-1 contributed to recognition by ubiquitin ligases, which mark phosphorylated IRAK-1 for proteasomal degradation (6, 31, 60). On the other hand, other investigators suggested that IRAK-1 is not degraded but is instead translocated to the nucleus upon IL-1 treatment, where it fulfills an unidentified function (3). Although the exact role of IRAK-1 degradation in IL-1 signaling is controversial, it is known that degradation of IRAK-1 leads to a shutdown of the IL-1 response and represents a negative feedback loop in the NF-κB pathway. So far, the precise mechanism of IRAK-1 ubiquitination and degradation has not been studied, but Tollip is a good candidate to bring the ubiquitination machinery into the proximity of IRAK-1 (25, 62). It is important to elucidate the metabolic pathways of IRAK-1 as well as Tollip following CD26-mediated caveolin-1 phosphorylation in future studies.

On the basis of our results and previously reported findings, we propose a model to describe the signaling events in monocytes triggered by CD26–caveolin-1 interaction (Fig. 8A). In this model, a part of N termini of caveolin-1 is exposed after tetanus toxoid is trafficked in monocytes (43), and CD26 induces aggregation and phosphorylation of caveolin-1 expressed in the T-cell–APC contact area as demonstrated in our previous report (43). Following caveolin-1 phosphorylation, dissociation of Tollip and IRAK-1 is induced with subsequent phosphorylation of IRAK in the cytosol. This sequence of events allows for activation of NF-κB and transcription of the CD86 gene. T cells then expand clonally and acquire additional effector functions as a result of CD26–caveolin-1 interaction as well as CD28-B7 and CD40-CD154 interaction (2, 29, 35). Consequently, T-cell proliferation that is dependent on the presence of CD26 is observed in response to recall antigen such as tetanus toxoid (Fig. 8B).

In endothelial cells (EC), inhibition of the scaffolding domain of caveolin-1 reduces inflammation by inhibition of endothelial nitric oxide synthetase, which is bound to caveolin-1 (4). Moreover, human EC in vivo express constitutively major histocompatibility (MHC) class II molecules and caveolin-1 (9, 51), whereas murine EC do not express MHC class II molecules (9). Thus, human EC have an ability to present antigens to $CD4^+$ T cells inducing proliferation of memory T cells (46) and play an important role in grafting of transplants (54) as well as in presenting recall antigens in human delayed hypersensitivity reactions (13, 46). In this regard, inhibition of caveolin-1 and CD26 interaction in the human system may provide a significant treatment strategy not only for the inflammatory state but also for transplantation. In the clinical setting, patients with autoimmune diseases such Graves' disease and rheumatoid arthritis have increased levels of $CD26^+$ T cells in inflamed tissues such as thyroid and synovial membrane and fluids (14, 37). In addition, enhancement of CD26 expression in these autoimmune diseases may correlate with disease severity (17, 40). Moreover, it has been shown that T cells migrating through endothelial cell monolayers in vitro express high levels of CD26 (33, 34), while the fact that chemokines play a key role in T-cell migration supports the notion that CD26/DPPIV may interact with these biological factors (23, 44, 47). These findings imply that $CD26^+$ T cells play a role in the inflammation process and subsequent tissue damage in autoimmune diseases. Our results may thus provide a new approach to the treatment of autoimmune diseases or other immune-mediated disorders by directly interfering with activated T-cell and APC interaction. Moreover, targeting the interaction of the pocket structure of CD26 and the scaffolding domain of caveolin-1 may lead to novel therapeutic approaches utilizing agonists or antagonists that regulate antigen-specific immune response in not only immune-mediated disorders but also cancer immunotherapy and viral vaccination as strategies to enhance immune response (8).

ACKNOWLEDGMENTS

This work was supported by a grant-in-aid of the Ministry of Education, Science, Sports, and Culture and the Ministry of Health, Labor, and Welfare, Japan (K.O. and C.M.). N.H.D. is the recipient of a grant from the MD Anderson Cancer Center Physician-Scientist Program and the Gillson Longenbaugh Foundation.

REFERENCES

1. **Abreu, M. T., P. Vora, E. Faure, L. S. Thomas, E. T. Arnold, and M. Arditi.** 2001. Decreased expression of Toll-like receptor-4 and MD-2 correlates with intestinal epithelial cell protection against dysregulated proinflammatory gene expression in response to bacterial lipopolysaccharide. J. Immunol. **167**:1609–1616.
2. **Berberich, I., G. L. Shu, and E. A. Clark.** 1994. Cross-linking CD40 on B cells rapidly activates nuclear factor-kappa B. J. Immunol. **153**:4357–4366.
3. **Böl, G., O. J. Kreuzer, and R. Brigelius-Flohe.** 2000. Translocation of the interleukin-1 receptor-associated kinase-1 (IRAK-1) into the nucleus. FEBS Lett. **477**:73–78.
4. **Bucci, M., J. P. Gratton, R. D. Rudic, L. Acevedo, F. Roviezzo, G. Cirino, and W. C. Sessa.** 2000. In vivo delivery of the caveolin-1 scaffolding domain inhibits nitric oxide synthesis and reduces inflammation. Nat. Med. **6**:1362–1367.
5. **Burns, K., J. Clatworthy, L. Martin, F. Martinon, C. Plumpton, B. Maschera, A. Lewis, K. Ray, J. Tschopp, and F. Volpe.** 2000. Tollip, a new component of the IL-1RI pathway, links IRAK to the IL-1 receptor. Nat. Cell Biol. **2**:346–351.

6. **Burns, K., S. Janssens, B. Brissoni, N. Olivos, R. Beyaert, and J. Tschopp.** 2003. Inhibition of interleukin 1 receptor/Toll-like receptor signaling through the alternatively spliced, short form of MyD88 is due to its failure to recruit IRAK-4. J. Exp. Med. **197**:263–268.
7. **Cao, Z., W. J. Henzel, and X. Gao.** 1996. IRAK: a kinase associated with the interleukin-1 receptor. Science **271**:1128–1131.
8. **Carver, L. A., and J. E. Schnitzer.** 2003. Caveolae: mining little caves for new cancer targets. Nat. Rev. Cancer **3**:571–581.
9. **Choo, J. K., J. D. Seebach, V. Nickeleit, A. Shimizu, H. Lei, D. H. Sachs, and J. C. Madsen.** 1997. Species differences in the expression of major histocompatibility complex class II antigens on coronary artery endothelium: implications for cell-mediated xenoreactivity. Transplantation **64**:1315–1322.
10. **Cooke, E. L., I. J. Uings, C. L. Xia, P. Woo, and K. P. Ray.** 2001. Functional analysis of the interleukin-1-receptor-associated kinase (IRAK-1) in interleukin-1 beta-stimulated nuclear factor kappa B (NF-kappa B) pathway activation: IRAK-1 associates with the NF-kappa B essential modulator (NEMO) upon receptor stimulation. Biochem. J. **359**:403–410.
11. **Dang, N. H., Y. Torimoto, K. Shimamura, T. Tanaka, J. F. Daley, S. F. Schlossman, and C. Morimoto.** 1991. 1F7 (CD26): a marker of thymic maturation involved in the differential regulation of the CD3 and CD2 pathways of human thymocyte activation. J. Immunol. **147**:2825–2832.
12. **Dang, N. H., Y. Torimoto, K. Sugita, J. F. Daley, P. Schow, C. Prado, S. F. Schlossman, and C. Morimoto.** 1990. Cell surface modulation of CD26 by anti-1F7 monoclonal antibody. Analysis of surface expression and human T cell activation. J. Immunol. **145**:3963–3971.
13. **Dumonde, D. C., M. S. Pulley, F. J. Paradinas, B. M. Southcott, D. O'Connell, M. R. Robinson, F. den Hollander, and A. H. Schuurs.** 1982. Histological features of skin reactions to human lymphoid cell line lymphokine in patients with advanced cancer. J. Pathol. **138**:289–308.
14. **Eguchi, K., Y. Ueki, C. Shimomura, T. Otsubo, H. Nakao, K. Migita, A. Kawakami, M. Matsunaga, H. Tezuka, N. Ishikawa, et al.** 1989. Increment in the Ta1+ cells in the peripheral blood and thyroid tissue of patients with Graves' disease. J. Immunol. **142**:4233–4240.
15. **Feng, X., M. L. Gaeta, L. A. Madge, J. H. Yang, J. R. Bradley, and J. S. Pober.** 2001. Caveolin-1 associates with TRAF2 to form a complex that is recruited to tumor necrosis factor receptors. J. Biol. Chem. **276**:8341–8349.
16. **Fleischer, B.** 1994. CD26: a surface protease involved in T-cell activation. Immunol. Today **15**:180–184.
17. **Gerli, R., C. Muscat, A. Bertotto, O. Bistoni, E. Agea, R. Tognellini, G. Fiorucci, M. Cesarotti, and S. Bombardieri.** 1996. CD26 surface molecule involvement in T cell activation and lymphokine synthesis in rheumatoid and other inflammatory synovitis. Clin. Immunol. Immunopathol. **80**:31–37.
18. **Glenney, J. R., Jr.** 1989. Tyrosine phosphorylation of a 22-kDa protein is correlated with transformation by Rous sarcoma virus. J. Biol. Chem. **264**: 20163–20166.
19. **Hegen, M., J. Kameoka, R. P. Dong, S. F. Schlossman, and C. Morimoto.** 1997. Cross-linking of CD26 by antibody induces tyrosine phosphorylation and activation of mitogen-activated protein kinase. Immunology **90**:257–264.
20. **Ikushima, H., Y. Munakata, T. Ishii, S. Iwata, M. Terashima, H. Tanaka, S. F. Schlossman, and C. Morimoto.** 2000. Internalization of CD26 by mannose 6-phosphate/insulin-like growth factor II receptor contributes to T cell activation. Proc. Natl. Acad. Sci. USA **97**:8439–8444.
21. **Ishii, T., K. Ohnuma, A. Murakami, N. Takasawa, S. Kobayashi, N. H. Dang, S. F. Schlossman, and C. Morimoto.** 2001. CD26-mediated signaling for T cell activation occurs in lipid rafts through its association with CD45RO. Proc. Natl. Acad. Sci. USA **98**:12138–12143.
22. **Ishii, T., K. Ohnuma, A. Murakami, N. Takasawa, T. Yamochi, S. Iwata, M. Uchiyama, N. H. Dang, H. Tanaka, and C. Morimoto.** 2003. SS-A/Ro52, an autoantigen involved in CD28-mediated IL-2 production. J. Immunol. **170**: 3653–3661.
23. **Iwata, S., N. Yamaguchi, Y. Munakata, H. Ikushima, J. F. Lee, O. Hosono, S. F. Schlossman, and C. Morimoto.** 1999. CD26/dipeptidyl peptidase IV differentially regulates the chemotaxis of T cells and monocytes toward RANTES: possible mechanism for the switch from innate to acquired immune response. Int. Immunol. **11**:417–426.
24. **Kanakaraj, P., P. H. Schafer, D. E. Cavender, Y. Wu, K. Ngo, P. F. Grealish, S. A. Wadsworth, P. A. Peterson, J. J. Siekierka, C. A. Harris, and W. P. Fung-Leung.** 1998. Interleukin (IL)-1 receptor-associated kinase (IRAK) requirement for optimal induction of multiple IL-1 signaling pathways and IL-6 production. J. Exp. Med. **187**:2073–2079.
25. **Katoh, Y., Y. Shiba, H. Mitsuhashi, Y. Yanagida, H. Takatsu, and K. Nakayama.** 2004. Tollip and Tom1 form a complex and recruit ubiquitin-conjugated proteins onto early endosomes. J. Biol. Chem. **279**:24435–24443.
26. **Kobayashi, K., L. D. Hernandez, J. E. Galan, C. A. Janeway, Jr., R. Medzhitov, and R. A. Flavell.** 2002. IRAK-M is a negative regulator of Toll-like receptor signaling. Cell **110**:191–202.
27. **Kobayashi, S., K. Ohnuma, M. Uchiyama, K. Iino, S. Iwata, N. H. Dang, and C. Morimoto.** 2004. Association of CD26 with CD45RA outside lipid rafts attenuates cord blood T-cell activation. Blood **103**:1002–1010.
28. **Lei, M. G., and D. C. Morrison.** 2000. Differential expression of caveolin-1 in lipopolysaccharide-activated murine macrophages. Infect. Immun. **68**:5084–5089.
29. **Lenschow, D. J., A. I. Sperling, M. P. Cooke, G. Freeman, L. Rhee, D. C. Decker, G. Gray, L. M. Nadler, C. C. Goodnow, and J. A. Bluestone.** 1994. Differential up-regulation of the B7-1 and B7-2 costimulatory molecules after Ig receptor engagement by antigen. J. Immunol. **153**:1990–1997.
30. **Li, T., J. Hu, and L. Li.** 2004. Characterization of Tollip protein upon lipopolysaccharide challenge. Mol. Immunol. **41**:85–92.
31. **Li, X., M. Commane, C. Burns, K. Vithalani, Z. Cao, and G. R. Stark.** 1999. Mutant cells that do not respond to interleukin-1 (IL-1) reveal a novel role for IL-1 receptor-associated kinase. Mol. Cell. Biol. **19**:4643–4652.
32. **Makino, Y., H. Nakamura, E. Ikeda, K. Ohnuma, K. Yamauchi, Y. Yabe, L. Poellinger, Y. Okada, C. Morimoto, and H. Tanaka.** 2003. Hypoxia-inducible factor regulates survival of antigen receptor-driven T cells. J. Immunol. **171**:6534–6540.
33. **Masuyama, J., J. S. Berman, W. W. Cruikshank, C. Morimoto, and D. M. Center.** 1992. Evidence for recent as well as long term activation of T cells migrating through endothelial cell monolayers in vitro. J. Immunol. **148**: 1367–1374.
34. **Masuyama, J., T. Yoshio, K. Suzuki, S. Kitagawa, M. Iwamoto, T. Kamimura, D. Hirata, A. Takeda, S. Kano, and S. Minota.** 1999. Characterization of the 4C8 antigen involved in transendothelial migration of CD26(hi) T cells after tight adhesion to human umbilical vein endothelial cell monolayers. J. Exp. Med. **189**:979–990.
35. **McAdam, A. J., A. N. Schweitzer, and A. H. Sharpe.** 1998. The role of B7 co-stimulation in activation and differentiation of CD4+ and CD8+ T cells. Immunol. Rev. **165**:231–247.
36. **Mestas, J., and C. C. Hughes.** 2004. Of mice and not men: differences between mouse and human immunology. J. Immunol. **172**:2731–2738.
37. **Mizokami, A., K. Eguchi, A. Kawakami, H. Ida, Y. Kawabe, T. Tsukada, T. Aoyagi, K. Maeda, C. Morimoto, and S. Nagataki.** 1996. Increased population of high fluorescence 1F7 (CD26) antigen on T cells in synovial fluid of patients with rheumatoid arthritis. J. Rheumatol. **23**:2022–2026.
38. **Morimoto, C., and S. F. Schlossman.** 1998. The structure and function of CD26 in the T-cell immune response. Immunol. Rev. **161**:55–70.
39. **Morimoto, C., Y. Torimoto, G. Levinson, C. E. Rudd, M. Schrieber, N. H. Dang, N. L. Letvin, and S. F. Schlossman.** 1989. 1F7, a novel cell surface molecule, involved in helper function of CD4 cells. J. Immunol. **143**:3430–3439.
40. **Muscat, C., A. Bertotto, E. Agea, O. Bistoni, R. Ercolani, R. Tognellini, F. Spinozzi, M. Cesarotti, and R. Gerli.** 1994. Expression and functional role of 1F7 (CD26) antigen on peripheral blood and synovial fluid T cells in rheumatoid arthritis patients. Clin. Exp. Immunol. **98**:252–256.
41. **Naquet, P., H. R. MacDonald, P. Brekelmans, J. Barbet, S. Marchetto, W. Van Ewijk, and M. Pierres.** 1988. A novel T cell-activating molecule (THAM) highly expressed on CD4−CD8− murine thymocytes. J. Immunol. **141**:4101–4109.
42. **Ohnuma, K., Y. Munakata, T. Ishii, S. Iwata, S. Kobayashi, O. Hosono, H. Kawasaki, N. H. Dang, and C. Morimoto.** 2001. Soluble CD26/dipeptidyl peptidase IV induces T cell proliferation through CD86 up-regulation on APCs. J. Immunol. **167**:6745–6755.
43. **Ohnuma, K., T. Yamochi, M. Uchiyama, K. Nishibashi, N. Yoshikawa, N. Shimizu, S. Iwata, H. Tanaka, N. H. Dang, and C. Morimoto.** 2004. CD26 up-regulates expression of CD86 on antigen-presenting cells by means of caveolin-1. Proc. Natl. Acad. Sci. USA **101**:14186–14191.
44. **Ohtsuki, T., O. Hosono, H. Kobayashi, Y. Munakata, A. Souta, T. Shioda, and C. Morimoto.** 1998. Negative regulation of the anti-human immunodeficiency virus and chemotactic activity of human stromal cell-derived factor 1alpha by CD26/dipeptidyl peptidase IV. FEBS Lett. **431**:236–240.
45. **Oravecz, T., M. Pall, G. Roderiquez, M. D. Gorrell, M. Ditto, N. Y. Nguyen, R. Boykins, E. Unsworth, and M. A. Norcross.** 1997. Regulation of the receptor specificity and function of the chemokine RANTES (regulated on activation, normal T cell expressed and secreted) by dipeptidyl peptidase IV (CD26)-mediated cleavage. J. Exp. Med. **186**:1865–1872.
46. **Pober, J. S., M. S. Kluger, and J. S. Schechner.** 2001. Human endothelial cell presentation of antigen and the homing of memory/effector T cells to skin. Ann. N. Y. Acad. Sci. **941**:12–25.
47. **Proost, P., S. Struyf, D. Schols, G. Opdenakker, S. Sozzani, P. Allavena, A. Mantovani, K. Augustyns, G. Bal, A. Haemers, A. M. Lambeir, S. Scharpe, J. Van Damme, and I. De Meester.** 1999. Truncation of macrophage-derived chemokine by CD26/dipeptidyl-peptidase IV beyond its predicted cleavage site affects chemotactic activity and CC chemokine receptor 4 interaction. J. Biol. Chem. **274**:3988–3993.
48. **Razani, B., S. E. Woodman, and M. P. Lisanti.** 2002. Caveolae: from cell biology to animal physiology. Pharmacol. Rev. **54**:431–467.
49. **Sargiacomo, M., P. E. Scherer, Z. Tang, E. Kubler, K. S. Song, M. C. Sanders, and M. P. Lisanti.** 1995. Oligomeric structure of caveolin: implications for caveolae membrane organization. Proc. Natl. Acad. Sci. USA **92**:9407–9411.
50. **Shih, S. C., G. Prag, S. A. Francis, M. A. Sutanto, J. H. Hurley, and L. Hicke.** 2003. A ubiquitin-binding motif required for intramolecular monoubiquitylation, the CUE domain. EMBO J. **22**:1273–1281.
51. **Smart, E. J., G. A. Graf, M. A. McNiven, W. C. Sessa, J. A. Engelman, P. E.**

Scherer, T. Okamoto, and M. P. Lisanti. 1999. Caveolins, liquid-ordered domains, and signal transduction. Mol. Cell. Biol. 19:7289–7304.
52. Song, K. S., Z. Tang, S. Li, and M. P. Lisanti. 1997. Mutational analysis of the properties of caveolin-1. A novel role for the C-terminal domain in mediating homo-typic caveolin-caveolin interactions. J. Biol. Chem. 272: 4398–4403.
53. Swantek, J. L., M. F. Tsen, M. H. Cobb, and J. A. Thomas. 2000. IL-1 receptor-associated kinase modulates host responsiveness to endotoxin. J. Immunol. 164:4301–4306.
54. Sykes, M. 2001. Mixed chimerism and transplant tolerance. Immunity 14: 417–424.
55. Tanaka, J., Y. Miwa, K. Miyoshi, A. Ueno, and H. Inoue. 1999. Construction of Epstein-Barr virus-based expression vector containing mini-oriP. Biochem. Biophys. Res. Commun. 264:938–943.
56. Tanaka, T., D. Camerini, B. Seed, Y. Torimoto, N. H. Dang, J. Kameoka, H. N. Dahlberg, S. F. Schlossman, and C. Morimoto. 1992. Cloning and functional expression of the T cell activation antigen CD26. J. Immunol. 149:481–486.
57. Tanaka, T., J. S. Duke-Cohan, J. Kameoka, A. Yaron, I. Lee, S. F. Schlossman, and C. Morimoto. 1994. Enhancement of antigen-induced T-cell proliferation by soluble CD26/dipeptidyl peptidase IV. Proc. Natl. Acad. Sci. USA 91:3082–3086.
58. Tanaka, T., J. Kameoka, A. Yaron, S. F. Schlossman, and C. Morimoto. 1993. The costimulatory activity of the CD26 antigen requires dipeptidyl peptidase IV enzymatic activity. Proc. Natl. Acad. Sci. USA 90:4586–4590.
59. Thomas, J. A., J. L. Allen, M. Tsen, T. Dubnicoff, J. Danao, X. C. Liao, Z. Cao, and S. A. Wasserman. 1999. Impaired cytokine signaling in mice lacking the IL-1 receptor-associated kinase. J. Immunol. 163:978–984.
60. Yamin, T. T., and D. K. Miller. 1997. The interleukin-1 receptor-associated kinase is degraded by proteasomes following its phosphorylation. J. Biol. Chem. 272:21540–21547.
61. Yamochi, T., I. Nishimoto, T. Okuda, and M. Matsuoka. 2001. ik3-1/Cables is associated with Trap and Pctaire2. Biochem. Biophys. Res. Commun. 286:1045–1050.
62. Zhang, G., and S. Ghosh. 2002. Negative regulation of Toll-like receptor-mediated signaling by Tollip. J. Biol. Chem. 277:7059–7065.

Nedd9 Protein, a Cas-L Homologue, Is Upregulated After Transient Global Ischemia in Rats

Possible Involvement of Nedd9 in the Differentiation of Neurons After Ischemia

Takahiro Sasaki, MD, PhD; Satoshi Iwata, MD, PhD; Hirotaka James Okano, MD, PhD; Yasuyo Urasaki, MS; Junichi Hamada, MD, PhD; Hirotoshi Tanaka, MD, PhD; Nam H. Dang, MD, PhD; Hideyuki Okano, MD, PhD; Chikao Morimoto, MD, PhD

Background and Purpose—Some proteins involved in self-repair after stroke in the adult brain are primarily expressed during embryonic development and strongly down-regulated during the early postnatal phase. Neuronal precursor cell-expressed, developmentally down-regulated gene (Nedd) 9 was recognized to be identical to Crk-associated substrate lymphocyte type (Cas-L), a docking protein that associates with a variety of signaling molecules, such as focal adhesion kinase (FAK), proline-rich tyrosine kinase 2 (Pyk2), and Crk. We investigated the involvement of these proteins in the pathophysiology of global cerebral ischemia.

Methods—The mouse Cas-L/Nedd9 cDNAs were cloned. The expression and function of Cas-L/Nedd9 protein in the pathogenesis of global ischemia in rats was investigated by RT-PCR, Western blot analysis, and immunohistochemistry. The neurite outgrowth of the transfectants of Nedd9 deletion mutants in PC-12 cells was also assessed to clarify the function of the Nedd9 protein.

Results—Nedd9 was a splicing variant of Cas-L and was selectively induced in neurons of the cerebral cortex and hippocampus 1 to 14 days after the ischemia. Induced Nedd9 protein was tyrosine phosphorylated and was bound to FAK in dendrite and soma of neurons after the ischemia. Finally, it was demonstrated that Nedd9 promoted neurite outgrowth of PC-12 cells.

Conclusions—Our study may support the potential of Nedd9 for participation in the differentiation of neurons after global ischemia in rats. (***Stroke.* 2005;36:2457-2462.)**

Key Words: cerebral ischemia ■ global ■ rats ■ neural differentiation

Identification of an endogenous protein involved in self-repair after stroke in adult brain can potentially widen the therapeutic time window. Ischemia is a powerful reformatting and reprogramming stimulus for the brain, which induces endogenous proteins related to the pathophysiology of the injured brain.[1] Some of these proteins, such as neurocan,[2] Nedd2/Caspase2,[3] and GAP43,[4] are primarily expressed by neurons or glia during embryonic development and are strongly down-regulated during the early postnatal phase.

Nedd9 was initially identified as a neuronal precursor cell (NPC)-expressed, developmentally down-regulated gene in the mouse central nervous system. Gene expression of Nedd9 is detected in the embryonic brain of embryonal day (E) 10 and 14 and disappears in the adult mouse brain.[5] The product of Nedd9 was subsequently reported to be identical to the mouse Crk-associated substrate lymphocyte-type (Cas-L) according to the homology database (http://www.ncbi.nlm.nih.gov/), which is also known as human enhancer of filamentation 1 cloned by another group.[6] Human Cas-L was first identified by our group as a 105-kDa protein predominantly tyrosine phosphorylated by the ligation of β1 integrins in human leukemia H9 cells.[7] The major biological functions of Cas-L are the restoration of interleukin-2 production by costimulation with β1 integrins and T-cell receptor complex[8] and the enhancement of cell migration by the engagement of β1 integrins and T-cell receptor complex or β1 integrins alone.[9] To exert these functions, it is necessary that Cas-L is associated with focal adhesion kinase (FAK) or proline-rich tyrosine kinase 2 (Pyk2) and is tyrosine phosphorylated by these kinases.[10] Cas-L is a hematopoietic variant of p130Cas,[7]

Received June 26, 2004; final revision received December 8, 2004; accepted January 11, 2005.

From the Division of Clinical Immunology (T.S., S.I., Y.U., H.T., C.M.), Advanced Clinical Research Center, Institute of Medical Science, the University of Tokyo, Tokyo, Japan; the Departments of Physiology (H.J.O., H.O.) and Neurology (T.S., J.H.), Keio University School of Medicine; Core Research for Evolutional Science and Technology (H.J.O., H.O.), Japan Science and Technology Agency, Saitama, Japan; and the Department of Lymphoma/Myeloma (N.H.D.), MD Anderson Cancer Center, University of Texas, TX.

Correspondence to Chikao Morimoto, MD, PhD, Division of Clinical Immunology, Advanced Clinical Research Center, the Institute of Medical Science, the University of Tokyo, 4-6-1 Shirokanedai, Minato-ku, Tokyo 108-8639, Japan. E-mail morimoto@ims.u-tokyo.ac.jp

Stroke is available at http://www.strokeaha.org

DOI: 10.1161/01.STR.0000185672.10390.30

which was identified as a 130-kDa protein that is highly tyrosine phosphorylated in v-Src-[11] and v-Crk-transformed cells.[12] These proteins and Efs/Sin compose the Cas family, which has a conserved secondary structure with numerous protein-protein interactions, such as Src-homology 3 (SH3) domain, substrate domain, serine-rich domain, coiled-coil regions, helix-loop-helix domain, and COOH-terminal domain.[7,13] These structures feature a docking molecule, which interacts with a variety of signaling molecules, including FAK and Pyk2. The function of Cas-L/Nedd9 in relation to the pathogenesis of brain ischemia, as well as the expression in adult brain, remains unknown.

In the present study, we cloned the cDNAs of mouse Cas-L/Nedd9 and assessed the temporal profile of Cas-L/Nedd9, as well as its related molecules, such as p130Cas, FAK, and Pyk2, in the brain of rats with transient global ischemia. We also investigated its physiological function by using PC-12 cells transfected with Nedd9.

Methods

Antibodies and Reagents

Monoclonal antibodies (mAbs) against FAK, p130Cas, and Pyk2 were obtained from Transduction Laboratories. Antiphosphotyrosine antibody (4G10) was purchased from Upstate Biotechnology, Inc. A mAb to neuron-specific nuclear protein (NeuN) was from Chemicon International, and horseradish peroxidase-conjugated goat anti-mouse and anti-goat anti-rabbit antibodies were from Promega. Affinity-purified rabbit anti-mouse antibody was purchased from Jackson Laboratories. Production of polyclonal antibody specific to Cas-L was described previously.[14] Protein A sepharose beads were from Pharmacia Biotech. All of the other reagents were purchased from Sigma-Aldrich unless otherwise stated.

cDNA Cloning of Murine Cas-L/Nedd9

A λgt11 human placenta cDNA library (Clontech Laboratories) was screened by hybridization with a ^{32}P-labeled probe for human Cas-L cDNA, which was labeled with [α-^{32}P] dCTP by the random primer labeling method, for 16 hours at 50°C in a solution of 50 mmol/L Tris-HCl, pH 7.5, 1 mol/L NaCl, 1% SDS, and 100 μg/mL sonicated salmon testis DNA, and then washed at 65°C in 0.1×SSC containing 1% SDS.[15] The hybridization-positive clones were sequenced by an ABI Dideoxy Terminator Cycle Sequencing kit.

Animals

Male Sprague-Dawley rats weighing 250 to 350 g were anesthetized by an IP injection of pentobarbital sodium (40 mg/kg). Twenty-one minutes of global ischemia were induced by occlusion of both common arteries with systemic hypotension <50 mm Hg.[16] The rectal temperature was continuously monitored and maintained at 37.0°C to 37.5°C with a thermostatically controlled heating pad. The experimental committee of Keio University approved the experimental protocol as meeting the experimental animal guidelines of Keio University School of Medicine.

RT-PCR

RT-PCR was performed using ISOGEN agent and BcaBEST RNA PCR kit (Takara Bio, Inc) with the following primers: forward 5′-AAATGTGGGCGAGGAAT-3′ for rat Nedd9, 5′-AGGGCTCATCTGACCAC-3′ for rat Cas-L, and reverse 5′-TGACTGGAGGGCTCTTG-3′ for both cDNAs. PCR cycles were as follows: 94°C, 1 minute; 55.6°C, 1 minute; and 72°C, 2 minutes (30 cycles).

Immunoprecipitation and Immunoblotting

Tissues of cerebral cortex and hippocampus were homogenized in suspension buffer (20 mmol/L HEPES-KOH, pH 7.5, 250 mmol/L sucrose, 10 mmol/L KCl, 1.5 mmol/L $MgCl_2$, 1 mmol/L EDTA, 1 mmol/L EGTA, 1 mmol/L dithiothreitol, 0.1 mmol/L phenylmethylsulfonyl fluoride, 2 μg/mL aprotinin, 10 μg/mL leupeptin, and 5 μg/mL pepstatin A). The lysates were immunoprecipitated with anti–Cas-L polyclonal antibody and protein A sepharose beads. The samples were separated by 8% SDS-PAGE and electrotransferred onto polyvinylidene difluoride membranes (Millipore). For immunoblotting, the primary antibodies and their dilutions were as follows: anti–Cas-L polyclonal antibody (1:2500), anti-Pyk2 mAb (1:2500), anti-FAK mAb (1:2000), anti p130Cas mAb (1:2500), and anti–β-actin mAb (1:5000).

Histological Examinations

Anesthetized rats were perfused transcardially with heparinized saline followed by 4% paraformaldehyde/PBS for tissue fixation, and paraffinized sections were made. The paraffinized sections (10 μm) were dewaxed and permeabilized with 0.1% Triton X-100/PBS and then blocked in 4% FBS/PBS. The primary antibodies and their dilutions were as follows: anti–Cas-L rabbit polyclonal antibody, 1:200; anti-FAK mAb, 1:200; and NeuN, 1:200. The sections were finally exposed to 0.025% diaminobenzidine and 0.075% H_2O_2 in PBS for 1 minute. For immunofluorescence staining, fluorescein isothiocyanate or Texas Red-conjugated anti-rabbit or anti-mouse IgG antibodies at 1:100 were used as the secondary antibody.

Gene Transfer Using Retrovirus

Retroviral gene transfer was carried out using the ping-pong infection method using Plat-E cells,[17] PT-67 cells (Clontech), and Fugene6 reagent (Roche Diagnostics) with pMX-Nedd9 wild type-IRES-GFP, pMX-Nedd9 SH3-IRES-GFP, pMX-Nedd9 F-IRES-GFP, pMX-Nedd9 δ SH3-IRES-GFP, pMX-Nedd9 δ SD-IRES-GFP, or pMX-IRES-GFP. The supernatants of PT-67 infected with each retrovirus were used to infect PC-12 cells.

Assessment of Neurite Outgrowth of PC-12 Cells

Infected PC-12 cells were cultured in DMEM plus 10% fetal calf serum and 5% horse serum. For the examination of neuritogenesis, 2.5×10^4 cells were seeded per 35-mm plate, grown overnight, and starved (0.5% FCS plus 0.5% horse serum) for 16 to 20 hours, then 50 ng/mL nerve growth factor (NGF) was added. After 6 days of stimulation, neurite length was measured on photographed fields containing 50 to 100 cells. Data were expressed in 2 ways: first, as the neurite length averaged over diameter of soma (bar diagrams; y axis=cell diameters); and second, as the number of neurites per cell. The level of statistical significance was assessed by ANOVA followed by Scheffé's post hoc test. Statistical significance was set at $P<0.01$.

Results

Cloning of Mouse Cas-L Revealed That Cas-L Was a Splicing Variant of Nedd9 With Identical Functional Domains

Using the cloned mouse Cas-L-related cDNAs, a sequence homology search was performed against the cDNA and genomic database. Nedd9 was found to share high degrees of homology with mouse Cas-L: 98.9% in nucleotide sequence and 98.6% in amino acid sequence (Figure 1a). An analysis of mouse genomic database revealed that Cas-L (MKYK-) was a splicing variant of Nedd9 (MWAR-), and the functional domains of these proteins were identical to each other. A homology search against a rat genomic database showed that the deduced amino acid sequences of mouse and rat Nedd9 were highly conserved between these species: 92.7% in the

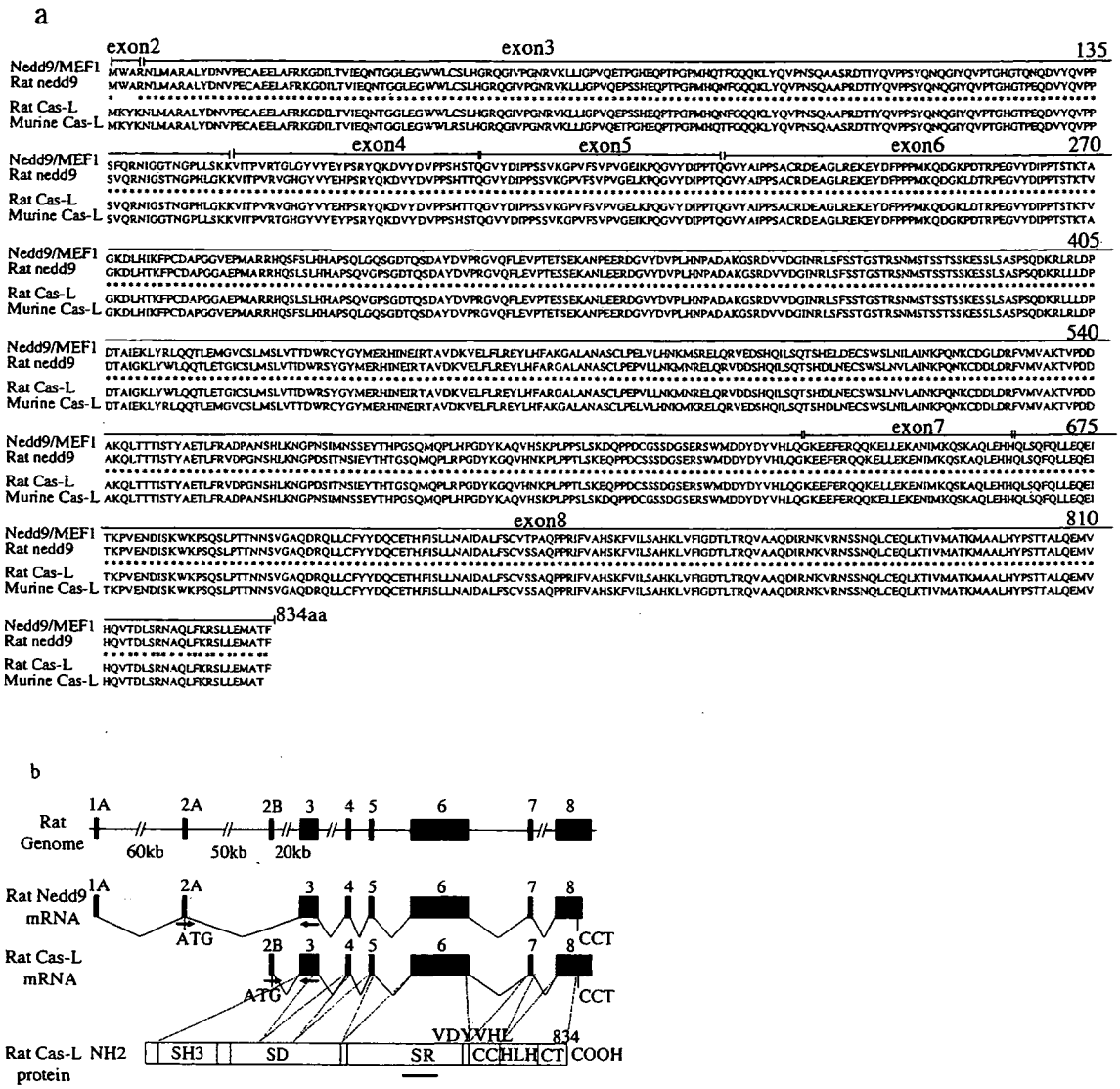

Figure 1. Nedd9 is a splicing variant of Cas-L. a, Comparison of the deduced amino acid sequences of Nedd9 and Cas-L from mouse and rat. b, Proposed model for the generation of Nedd9 and Cas-L mRNA variants and the multiple domain structure of Cas-L/Nedd9. Top, Organization of the Cas-L/Nedd9 gene. Exons are indicated by black boxes and numbered. Middle, The presence of exons in the different mRNAs represented by boxes linked by connecting lines. Translation initiation sites in exons 2A and 2B and the translation stop site in exon 8 are indicated. Arrows indicate the primer sites for PCR amplification designed to give products from Nedd9 mRNA and Cas-L mRNA, respectively. Bottom, The domain structure of Cas-L/Nedd9 is demonstrated. Bar indicates the responsible domain to be recognized by anti-Cas-L antibody used in this study. CC indicates coiled-coil regions; HLH, helix-loop-helix domain; CT, COOH-terminal region.

nucleotide sequence and 93.3% in the amino acid sequence, respectively. Rat Nedd9 shared high degrees of homology with rat Cas-L, 99.8% in nucleotide sequence and 99.8% in amino acid sequence (Figure 1a and 1b).

Nedd9, Not Cas-L, Was Transcriptionally Upregulated and Tyrosine Phosphorylated, Along With FAK in Cerebral Cortex and Hippocampus After Transient Global Ischemia

The Table shows the physiological parameters just before the induction of ischemia. There were no significant differences in the parameters among the groups, demonstrating that all of the rats used in the ischemia study had no significant difference in their condition. Expression of Nedd9 and Cas-L mRNAs in rats with global ischemia was analyzed by RT-PCR at 1, 3, 5, 7, or 14 days after 21-minute ischemia or at 1 hour after the sham operation. The RT-PCR assay was performed using a set of primers that amplifies the fragments of 203 and 225 bp from rat Nedd9 mRNA and Cas-L mRNA, respectively (Figure 1b). The expression of Nedd9 mRNA

Physiological Parameters Before the Induction of Ischemia

Day of Sacrifice	pH	Pao_2, mm Hg	$Paco_2$, mm Hg
Sham operation	7.415±0.022	73.1±2.2	35.8±2.9
1 day after ischemia	7.445±0.011	84.7±3.8	38.3±3.0
3 days after ischemia	7.442±0.003	77.0±3.1	39.0±1.9
5 days after ischemia	7.409±0.014	84.9±2.4	38.9±2.6
7 days after ischemia	7.437±0.023	90.7±4.7	37.9±4.6
14 days after ischemia	7.449±0.019	84.8±6.1	40.2±1.8

Mean±SEM. Physiological parameters did not differ among rats before induction of transient global ischemia. N=5.

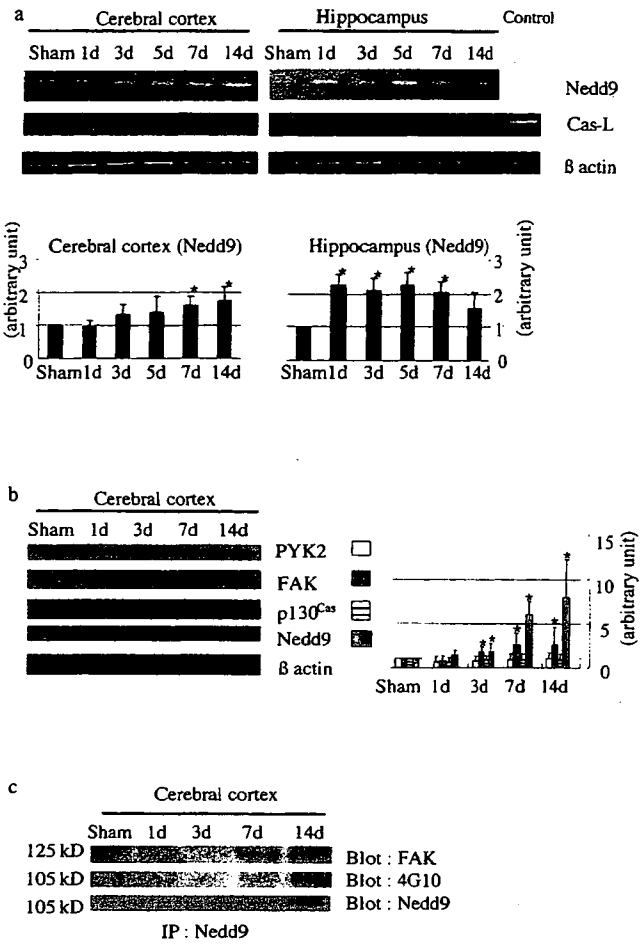

Figure 2. Nedd9 is preferentially upregulated with FAK and tyrosine-phosphorylated after transient global ischemia. a, A representative result of RT-PCR discriminating the 2 splicing variants of Cas-L/Nedd9 with β-actin as an internal control. Spleen of rats serves as positive control of Cas-L. b, The expression of proteins related to Cas-L/Nedd9 by immunoblotting. c, Nedd9 was immunoprecipitated at the indicated days after ischemia. Statistical significance is tested with respect to sham operated controls (*$P<0.001$).

was upregulated in both the cerebral cortex and hippocampus ≈1 to 14 days after ischemia, whereas the expression of Cas-L mRNA was not observed (Figure 2a).

In order to address the Cas-L/Nedd9-mediated signal transduction pathway, we examined the expression of other proteins, such as FAK, Pyk2, and p130Cas. Expression of Nedd9 protein and FAK was upregulated in a similar time course, whereas others did not show significant changes (Figure 2b). Furthermore, Nedd9 and FAK were coimmunoprecipitated at 3, 7, or 14 days after transient global ischemia. The immunoprecipitates were also blotted with the antiphosphotyrosine antibody, because activated Cas-L/Nedd9 is known to be tyrosine phosphorylated. Hence, our data demonstrated that Nedd9 was tyrosine-phosphorylated with similar kinetics as observed with protein levels of Nedd9.

Induced Nedd9 Was Localized in Dendrite-Like Structure and Cytosol of Neurons in Cerebral Cortex and Hippocampus

Nedd9- and FAK-immunoreactive cells were detected at the cerebral cortex and hippocampus 3 and 7 days after the ischemic insult but not detected at those of sham-operated rats. The expression pattern of these proteins 3 and 7 days after the ischemia were identical to each other (Figure 3a; data not shown). The rat cerebral cortex and hippocampal

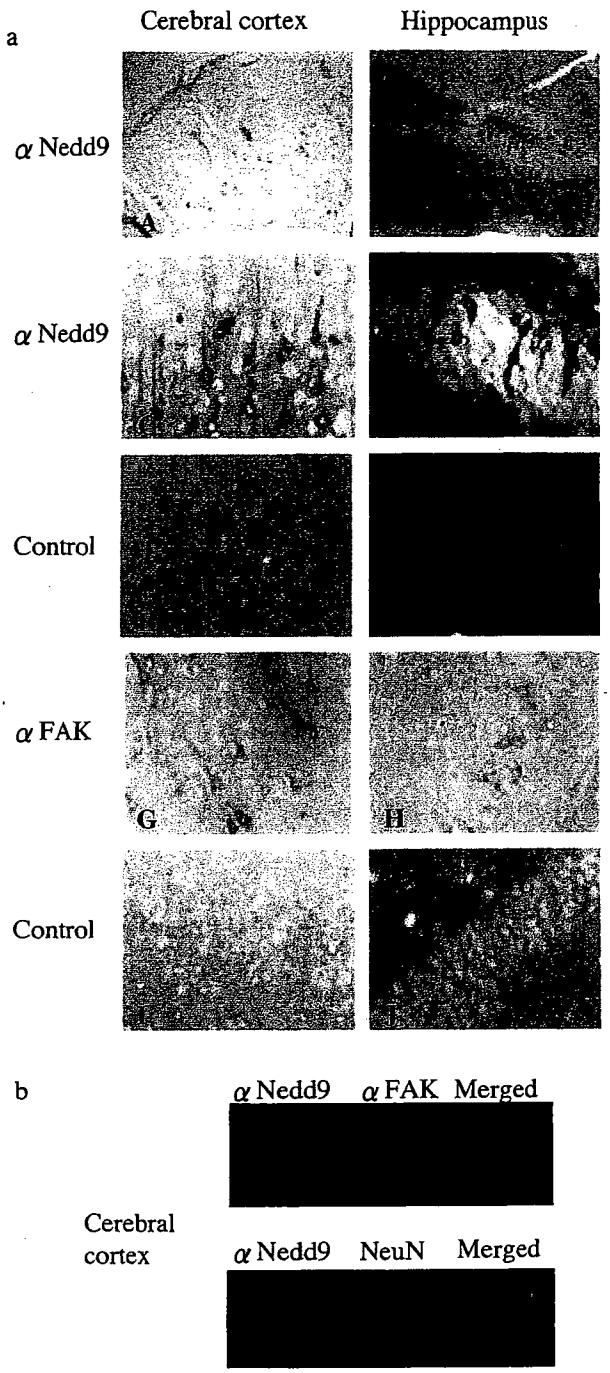

Figure 3. Induced Nedd9 protein is localized in dendrite-like structure and cytosol of neurons in the cerebral cortex and hippocampus. a, Representative figures of Nedd9 and FAK-immunoreactive cells detected at the cerebral cortex and hippocampus 7 days after transient global ischemia. Rat cerebral cortex and hippocampal coronal slices reveal intense Nedd9 and FAK immunoreactivity in the neuronal dendrites. In contrast, the neuronal cell nucleus appeared devoid of Nedd9 and FAK staining. A, C, E, G, and I, cerebral cortex; B, D, F, H, and J, hippocampus; A through D, anti-Nedd9 pAb; E and F, control; G and H, anti-FAK mAb; I and J, control; A and B, ischemia (×100); C through F and G through J, ischemia (×400); b, colocalization of Nedd9 and NeuN or FAK (×200).

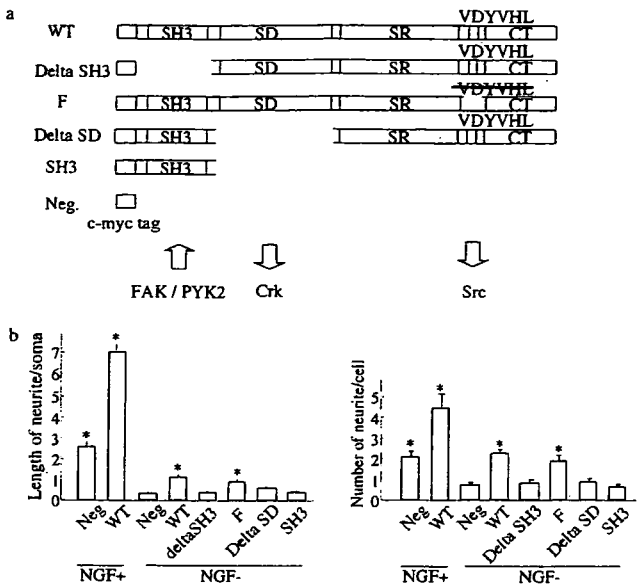

Figure 4. Nedd9 induces neurite outgrowth of PC-12 cells in the presence or absence of NGF. a, Nedd9 deletion mutants are shown. WT indicates wild type; SD, substrate domain; F, YDYVHL motif was mutated to FDFVHL; SR, serine-rich domain; CC, coiled-coil regions; HLH, helix-loop-helix domain; CT, COOH-terminal region. b, Neurite formation in the absence or presence of NGF. Data are expressed as neurite length averaged over diameter of soma (bar diagrams; *y* axis=cell diameters) and as number of neurites per cell. Statistical significance is tested with respect to unstimulated control PC-12 cells (*$P<0.001$).

coronal slices revealed intense Nedd9 immunoreactivity in the dendrite-like structures and cytosol. In contrast, the nucleus appeared devoid of Nedd9 staining. Colocalization of Nedd9 protein and FAK or NeuN confirmed the fact that Nedd9 protein was expressed in FAK-positive neurons (Figure 3b).

Nedd9 Promoted Neuronal Outgrowth of PC-12 Cells in the Presence or Absence of NGF

In order to clarify the physiological role of Nedd9, we examined the effect of Nedd9 on neurite outgrowth in PC-12 cells. Because we preliminarily found that the Nedd9 protein was expressed in neurons undergoing differentiation in the mouse embryonic neuroseptum and neurosphere (T. Sasaki, MD, PhD, unpublished data, 2003), we hypothesized that Nedd9 might play a role in neuronal differentiation. The rat pheochromocytoma PC-12 cells have been used for molecular analysis of the signaling pathways that lead to differentiation of peripheral nervous system neurons. Recently, this cell line was widely used for assays of regulatory factors expressed during central nervous system development.[18] PC-12 cells were infected with recombinant retrovirus to express myc-tagged Nedd9 and its mutants (Figure 4a). In contrast to cells infected with empty vector and mutants such as δSH3, SH3, and δSD, those expressing wild-type Nedd9 and mutant F showed promotion of neurite genesis in the presence or absence of NGF after 6 days of the addition of NGF or vehicle (Figure 4b). These findings suggest that Nedd9 may contribute to the promotion of neuronal differentiation of PC-12 cells.

Discussion

In this study, we have shown that Nedd9 is a splicing variant of Cas-L and is transcriptionally upregulated in the dendrites and cytosol of neurons in the cerebral cortex and hippocampus from 1 to 14 days after global ischemia in rats. We have also found that Nedd9 promotes neurite outgrowth of PC-12 cells. These data demonstrate that Nedd9, which is upregulated transiently during neuronal development and disappears in the adult brain, is reupregulated for neuronal differentiation after ischemia.

This is the first report to demonstrate that Cas-L and Nedd9 are splicing variants. The genetic difference between Cas-L and Nedd9 involves just 3 amino acids in the NH_2-terminus (Figure 1a): MKYK and MWAR, respectively. The fact that only Nedd9, but not Cas-L, expression is induced in response to ischemia recapitulates the physiological role of Nedd9, because it is expressed in NPCs during brain development (Figure 2a). The difference in expression between Nedd9 and Cas-L in the brain may be because of the transactivation of the Nedd9 gene mediated by nuclear factor κB, heat shock factor 1, or other related transcription factors known to be induced gradually after ischemia, because their binding sites exist in the upstream region of the rat Nedd9 gene. The molecular mechanism of Nedd9 gene regulation in these neurons will be an important subject for additional studies.

This is the first report to identify the expression of Nedd9 in the adult brain. In the focal ischemia model of mice, upregulation of several genes has been investigated and grouped as temporal episodes or "waves" of expression of different groups of genes.[1] Later waves of new gene expression, like Nedd9, include mediators that appear to be important in tissue remodeling and recovery of functions,[19] such as TGF-β[20] and osteopontin.[21] In this study, Nedd9 was selectively induced and tyrosine-phosphorylated in neurons of the cerebral cortex and hippocampus 1 to 14 days after transient global ischemia (Figures 2b and 2c and 3a and 3b). The regional difference of temporal expression of those proteins may be because of the different response to ischemic insult between the cerebral cortex and hippocampus. Those results led us to postulate that Nedd9 is required for neuronal differentiation, being primarily expressed in the embryonic brain but not in the fully differentiated adult neurons. Recently, it has been reported that stroke increases cell proliferation, with stroke-generated new neurons, as well as neuroblasts already formed before the insult, migrating into the damaged area.[22] These cells undergo differentiation and repair the neuronal network as short, remodeled neurons. The upregulation of Nedd9 in the adult brain appears to play a role in differentiation of neurons after ischemia.

To test the above hypothesis, we investigated the physiological function of Nedd9 in neurite outgrowth of PC-12 cells. We demonstrated that Nedd9 had a great impact on neurite outgrowth in the presence or absence of NGF when overexpressed in PC-12 cells. The fact that expression of δSH3, SH3, and δSD (substrate domain) inhibited neurite outgrowth is compatible with the role of the functional components of Nedd9, because Cas-L/Nedd9 bind to FAK through their SH3 domains,[6] and substrate domain is required for interaction with downstream SH2-containing proteins,

such as Crk, Nck, and SH-PTP2. Crk has been reported to induce differentiation of PC-12 in an NGF-independent manner.[23] These results, thus, confirm the hypothesis that delayed expression of Nedd9 and FAK may contribute to differentiation of neurons after ischemic injury in brain. We need to additionally investigate the role of Nedd9 in vivo, because PC-12 cells are not terminally differentiated in the setting used in the present study.

The source of Nedd9-positive neurons in ischemic brain should be investigated in future studies for its potential application to clinical treatment. It has been shown that some pathological conditions, such as ischemia, induce neurogenesis in the adult mammalian brain.[24,25] Even if Nedd9-positive neurons are derived from NPCs or have existed since the occurrence of ischemic insult, Nedd9 may be required to facilitate these regenerative or differentiating processes. The overexpression of Nedd9 may lead to a widening of the therapeutic time window for cerebral ischemia, particularly in the later phase of a stroke. In conclusion, our study may support the potential of Nedd9 for participation in the differentiation of neurons after global ischemia in rats.

Acknowledgments

This work was supported by National Institutes of Health grant AR33713; in part by grants-in-aid from the Ministry of Education, Science, and Culture and Ministry of Health, Labor and Welfare of Japan (H.O. and C.M.); and a grant from the Keio Medical Association and grants from the 21st Century COE Program of the Ministry of Education, Science and Culture of Japan to Keio University. We wish to thank Dr Toshio Kitamura for retroviral vector pMX-IRES-GFP and packaging cell line Plat-E. We appreciate the advice and expertise of Drs Kenjiro Kamiguchi, Department of Pathology at Sapporo Medical University; Mamoru Shibata, Department of Neurology; Shinnosuke Shibata, Department of Physiology at Keio University School of Medicine; and Seiji Kobayashi; as well as Akiko Souta-Kurihara. We also wish to thank Fumiki Nojima for excellent secretarial assistance.

References

1. Barone FC, Feuerstein GZ. Inflammatory mediators and stroke: new opportunities for novel therapeutics. *J Cereb Blood Flow Metab.* 1999; 19:819–834.
2. Haas CA, Rauch U, Thon N, Merten T, Deller T. Entorhinal cortex lesion in adult rats induces the expression of the neuronal chondroitin sulfate proteoglycan neurocan in reactive astrocytes. *J Neurosci.* 1999;19: 9953–9963.
3. Kinoshita M, Tomimoto H, Kinoshita A, Kumar S, Noda M. Up-regulation of the Nedd2 gene encoding an ICE/Ced-3-like cysteine protease in the gerbil brain after transient global ischemia. *J Cereb Blood Flow Metab.* 1997;17:507–514.
4. Yamada K, Goto S, Oyama T, Inoue N, Nagahiro S, Ushio Y. In vivo induction of the growth associated protein GAP43/B-50 in rat astrocytes following transient middle cerebral artery occlusion. *Acta Neuropathol (Berl).* 1994;88:553–557.
5. Kumar S, Tomooka Y, Noda M. Identification of a set of genes with developmentally down-regulated expression in the mouse brain. *Biochem Biophys Res Commun.* 1992;185:1155–1161.
6. Law SF, Estojak J, Wang B, Mysliwiec T, Kruh G, Golemis EA. Human enhancer of filamentation 1, a novel p130cas-like docking protein, associates with focal adhesion kinase and induces pseudohyphal growth in Saccharomyces cerevisiae. *Mol Cell Biol.* 1996;16:3327–3337.
7. Minegishi M, Tachibana K, Sato T, Iwata S, Nojima Y, Morimoto C. Structure and function of Cas-L, a 105-kD Crk-associated substrate-related protein that is involved in beta 1 integrin-mediated signaling in lymphocytes. *J Exp Med.* 1996;184:1365–1375.
8. Kamiguchi K, Tachibana K, Iwata S, Ohashi Y, Morimoto C. Cas-L is required for beta 1 integrin-mediated costimulation in human T cells. *J Immunol.* 1999;163:563–568.
9. Ohashi Y, Iwata S, Kamiguchi K, Morimoto C. Tyrosine phosphorylation of Crk-associated substrate lymphocyte-type is a critical element in TCR- and beta 1 integrin-induced T lymphocyte migration. *J Immunol.* 1999; 163:3727–3734.
10. Tachibana K, Urano T, Fujita H, Ohashi Y, Kamiguchi K, Iwata S, Hirai H, Morimoto C. Tyrosine phosphorylation of Crk-associated substrates by focal adhesion kinase. A putative mechanism for the integrin-mediated tyrosine phosphorylation of Crk-associated substrates. *J Biol Chem.* 1997; 272:29083–29090.
11. Reynolds AB, Kanner SB, Wang HC, Parsons JT. Stable association of activated pp60src with two tyrosine-phosphorylated cellular proteins. *Mol Cell Biol.* 1989;9:3951–3958.
12. Sakai R, Iwamatsu A, Hirano N, Ogawa S, Tanaka T, Mano H, Yazaki Y, Hirai H. A novel signaling molecule, p130, forms stable complexes in vivo with v-Crk and v-Src in a tyrosine phosphorylation-dependent manner. *EMBO J.* 1994;13:3748–3756.
13. O'Neill GM, Fashena SJ, Golemis EA. Integrin signalling: a new Cas(t) of characters enters the stage. *Trends Cell Biol.* 2000;10:111–119.
14. Ohashi Y, Tachibana K, Kamiguchi K, Fujita H, Morimoto C. T cell receptor-mediated tyrosine phosphorylation of Cas-L, a 105-kDa Crk-associated substrate-related protein, and its association of Crk and C3G. *J Biol Chem.* 1998;273:6446–6451.
15. Feinberg AP, Vogelstein B. A technique for radiolabeling DNA restriction endonuclease fragments to high specific activity. *Anal Biochem.* 1983;132:6–13.
16. Smith ML, Bendek G, Dahlgren N, Rosén I, Wieloch T, Siesjö BK. Models for studying long-term recovery following forebrain ischemia in the rat. 2. A 2-vessel occlusion model. *Acta Neurol Scand.* 1984;69: 385–401.
17. Gojo S, Kitamura S, Germeraad WT, Yoshida Y, Niwaya K, Kawachi K. Ex vivo gene transfer into myocardium using replication-defective retrovirus. *Cell Transplantation.* 1996;5:S81–S84.
18. Akamatsu W, Okano HJ, Osumi N, Inoue T, Nakamura S, Sakakibara S, Miura M, Matsuo N, Darnell RB, Okano H. Mammalian ELAV-like neuronal RNA-binding proteins HuB and HuC promote neuronal development in both the central and the peripheral nervous systems. *Proc Natl Acad Sci U S A.* 1999;96:9885–9890.
19. Read SJ, Parsons AA, Harrison DC, Philpott K, Kabnick K, O'Brien S, Clark S, Brawner M, Bates S, Gloger I, Legos JJ, Barone FC. Stroke genomics: approaches to identify, validate, and understand ischemic stroke gene expression. *J Cereb Blood Flow Metab.* 2001;21:755–778.
20. Wang X, Yue TL, White RF, Barone FC, Feuerstein GZ. Transforming growth factor-beta 1 exhibits delayed gene expression following focal cerebral ischemia. *Brain Res Bull.* 1995;36:607–609.
21. Wang X, Louden C, Yue TL, Ellison JA, Barone FC, Solleveld HA, Feuerstein GZ. Delayed expression of osteopontin after focal stroke in the rat. *J Neurosci.* 1998;18:2075–2083.
22. Arvidsson A, Collin T, Kirik D, Kokaia Z, Lindvall O. Neuronal replacement from endogenous precursors in the adult brain after stroke. *Natural Medicines.* 2002;8:963–970.
23. Tanaka S, Hattori S, Kurata T, Nagashima K, Fukui Y, Nakamura S, Matsuda M. Both the SH2 and SH3 domains of human CRK protein are required for neuronal differentiation of PC12 cells. *Mol Cell Biol.* 1993; 13:4409–4415.
24. Liu J, Solway K, Messing RO, Sharp FR. Increased neurogenesis in the dentate gyrus after transient global ischemia in gerbils. *J Neurosci.* 1998;18:7768–7778.
25. Yagita Y, Kitagawa K, Ohtsuki T, Takasawa K, Miyata T, Okano H, Hori M, Matsumoto M. Neurogenesis by progenitor cells in the ischemic adult rat hippocampus. *Stroke.* 2001;32:1890–1896.

Roxithromycin Specifically Inhibits Development of Collagen Induced Arthritis and Production of Proinflammatory Cytokines by Human T Cells and Macrophages

YASUYO URASAKI, MAMORU NORI, SATOSHI IWATA, TAKAHIRO SASAKI, OSAMU HOSONO, HIROSHI KAWASAKI, HIROTOSHI TANAKA, NAM H. DANG, EIJI IKEDA, and CHIKAO MORIMOTO

ABSTRACT. ***Objective.*** Roxithromycin (RXM) is a macrolide antibiotic that is effective in treatment of chronic lower respiratory tract diseases including diffuse panbronchiolitis and bronchial asthma. Its mechanism of action apart from its antibacterial action remains unclear. To determine the mechanism of action of RXM, we evaluated the effect of RXM on T cell functions and the inflammatory responses in mice with collagen induced arthritis (CIA).

Methods. T cell proliferation, cytokine production by T cells stimulated through CD28, CD26, or PMA with or without anti-CD3 Mab, cytokine production by macrophages stimulated with lipopolysaccharide, and transendothelial migration of T cells were analyzed in the presence or absence of various concentrations of RXM. We evaluated the effect of RXM treatment in collagen induced arthritis in mice.

Results. RXM did not affect the production of Th1-type and Th2-type cytokines, whereas it specifically inhibited production of proinflammatory cytokines such as tumor necrosis factor-α and interleukin 6 (IL-6) by T cells and macrophages. RXM inhibited T cell migration. We found that RXM treatment of mice with CIA reduced the severity of arthritis and serum level of IL-6, as well as leukocyte migration into the affected joints and destruction of bones and cartilage.

Conclusion. Our findings strongly suggest that RXM may be useful for the therapy of rheumatoid arthritis as well as other inflammatory diseases such as Crohn's disease. (J Rheumatol 2005; 32:1765–74)

Key Indexing Terms:
ROXITHROMYCIN PROINFLAMMATORY CYTOKINE T CELLS COSTIMULATION COLLAGEN INDUCED ARTHRITIS MACROPHAGES RHEUMATOID ARTHRITIS

There is increasing evidence that macrolides have a variety of biologic activities apart from their antibacterial actions[1]. Recently, low dose and longterm erythromycin treatment was shown to be effective in chronic lower respiratory tract disease, including diffuse panbronchiolitis and bronchial asthma[2,3], but the mechanism of action of this drug remains unclear. Erythromycin may have antiinflammatory properties, in addition to its antimicrobial effects. These immunomodulatory effects are reported to be the result of leukocyte activation, such as stimulation of phagocytosis[4,5], natural killer cell activity[5,6], production of superoxide anion[5], and neutrophil chemotaxis[2,7-9]. Roxithromycin (RXM), a new macrolide antibiotic, has a 14-member macrocycline ring structure resembling that of erythromycin[10]. RXM is characterized by rapid and complete absorption after oral administration, resulting in high serum concentrations[11]. *In vitro* investigation revealed that RXM modifies the function of neutrophils[12] and keratinocytes[13]. RXM also affects lymphocyte functions including proliferation induced by mitogens and purified protein derivative[14], as well as proliferation and cytokine secretion induced by mitogens[10,15].

In the initial stage of immune response, a certain antigen would be engaged by the T cell receptors, followed by

From the Division of Clinical Immunology, Advanced Clinical Research Center, Institute of Medical Science, University of Tokyo; Department of Lymphoma/Myeloma, M.D. Anderson Cancer Center, Houston, Texas, USA; and Department of Pathology, Keio University School of Medicine, Tokyo, Japan.

Supported by grants-in-aid from the Ministry of Education, Culture, Sports, Science and Technology and the Ministry of Health, Labor and Welfare of Japan.

Y. Urasaki, MS; M. Nori, MD; S. Iwata, MD; T. Sasaki, MD; O. Hosono, MD; H. Kawasaki, MD; H. Tanaka, MD, Division of Clinical Immunology, Advanced Clinical Research Center, Institute of Medical Science, University of Tokyo; N.H. Dang, MD, M.D. Anderson Cancer Center; E. Ikeda, MD, Department of Pathology, Keio University School of Medicine; C. Morimoto, MD, Division of Clinical Immunology, Advanced Clinical Research Center, Institute of Medical Science, University of Tokyo.

Address reprint requests to Dr. C. Morimoto, Division of Clinical Immunology, Advanced Clinical Research Center, Institute of Medical Science, University of Tokyo, 4-6-1 Shirokanedai, Minato-ku, Tokyo, 108-8639 Japan. E-mail: morimoto@ims.u-tokyo.ac.jp

Accepted for publication April 1, 2005.

release of various cytokines. However, this process alone is not sufficient for induction of all events that accompany T cell activation. Accumulating evidence suggests the presence of so-called costimulatory signals that occur through additional T cell surface molecules, which are independent of the CD3/T cell receptors[16]. These costimulatory signals are indispensable for full activation of T cells, which is characterized by T cell proliferation and cytokine production. Triggering of costimulatory signals therefore plays an important role in the generation of hypersensitive immune reaction. These costimulatory signals can be provided by a number of accessory molecules such as CD28/CTLA-4[17,18]. In addition, we identified CD26 as a novel costimulatory molecule that is preferentially expressed on CD4+ memory T cells[19-21] and that is speculated to be involved in the functions of effector T cells that migrate to inflammatory sites in immune mediated diseases[22].

In our study, we employed the costimulatory system of peripheral T cells *in vitro* to elucidate the immunomodulatory effect of RXM. We evaluated the therapeutic effect of RXM *in vivo* using the mouse model of rheumatoid arthritis (RA).

MATERIALS AND METHODS

Cells and reagents. Human peripheral blood mononuclear cells were isolated from healthy volunteer donors by Ficoll-Hypaque (Pharmacia Biotech, Piscataway, NJ, USA) density gradient centrifugation[19]. Unfractionated mononuclear cells were separated into an E rosette-positive (E+) population and were used as resting T cells. Monocytes were depleted by adherence to plastic plates for 24 h at 37°C followed by incubation with 5 mM L-leucine methyl ester HCl (Sigma Chemical Co., St. Louis, MO, USA) for 1 h. The monoclonal antibody (Mab) OKT3 was obtained from the American Tissue Culture Collection (ATCC; Rockville, MD, USA). Anti-CD26 (1F7) and the anti-CD28 Mab 4B10 were developed in our laboratory as described[18,19]. RXM (generously supplied by Eisai Ltd., Tokyo, Japan) was dissolved in DMSO and further diluted in the culture media consisting of RPMI-1640 and 10% fetal calf serum (FCS).

T cell proliferation assays. One hundred microliters of phosphate buffered saline containing 0.05 μg/ml of OKT3 in the presence or absence of 5 μg/ml of 1F7 (anti-CD26), or 5 μg/ml of 4B10 (anti-CD28) Mab, and incubated overnight at 4°C, as described[20]. Highly purified T cells were resuspended at 1×10^5 cells in 200 μl of RPMI-1640 medium containing 10% FCS, along with 4 different concentrations of RXM (0, 1.4, 14, and 28 μM). To assess PMA stimulation, the cell suspension supplemented with 5 ng/ml of PMA was applied into OKT3-coated wells. Cells were incubated at 37°C in a 5% CO_2 humidified atmosphere for 3 days. Cells were pulsed with 1 μCi/well of ^{3}H-thymidine (ICN Radiochemicals, Irvine, CA, USA) 8 h prior to harvest onto a glass-fiber filter (Wallac, Turku, Finland), and the incorporated radioactivity was quantified by a liquid scintillation counter (Wallac).

Cytokine production assays. Antibody-coated plates and purified T cells were prepared in the manner described above, with the exception of OKT3 concentration being 0.5 μg/ml. Cytokine production by T cells was assayed in triplicates in 96-well, flat-bottomplates as described above. After 24 h incubation, culture supernatants were subjected to ELISA [interleukin 2 (IL-2) and IL-4: Biosource International, Camarillo, CA, USA; interferon-γ (IFN-γ) and IL-5: R&D Systems, Minneapolis, MN, USA] to measure the levels of IL-2, IFN-γ, IL-4, and IL-5 as well as tumor necrosis factor-α (TNF-α) and IL-6. For TNF-α and IL-6 production by macrophages, macrophages were enriched from E-rosette-negative cells by adherence to plastic plates. Macrophages (1×10^6/ml) were suspended in 10% FCS-RPMI-1640 and stimulated with 1 μg/ml lipopolysaccharide (LPS; Sigma). After 8 h culture, supernatants were harvested and were subjected to ELISA (TNF-α and IL-6; R&D Systems). The serum levels of IL-6, TNF-α, IFN-γ, and IL-4 were also detected using an ELISA kit as described.

Assessment of cell viability. The trypan blue dye exclusion test was used to assess cell viability. In all experiments, the viability was found to be > 95% at each point measured (data not shown).

Transendothelial migration assay. Transendothelial migration activity was assessed using a kind of Boyden-chamber assay as described[23] with modifications. Human umbilical vein endothelial cells (HUVEC) obtained from ATCC were precultured to make a monolayer sheet on Transwell cell culture inserts with 3.0 μm pore size (Corning Costar, Cambridge, MA, USA) for 48 h. RXM was first dissolved in DMSO and further diluted in the assay medium consisting of RPMI-1640 and 0.6% bovine serum albumin, then added to culture plates in a final volume of 600 μl (the lower chamber) just before the migration assay. PHA-activated T cells (1×10^6 cells/well) were added to each insert in a volume of 200 μl simultaneously with the same concentration of RXM as in the corresponding culture wells (the upper chamber). Spontaneous migration (chemokinesis) assay was performed at 37°C for 8 h in the presence or absence of RXM, then harvested and counted by flow cytometry (FACS Calibur, Nippon Becton-Dickinson, Tokyo, Japan) for 1 min.

Induction of CIA. Male DBA/1J mice were purchased from Japan Charles River Breeding Laboratories (Tokyo, Japan). Bovine type II collagen (Collagen Research Center, Tokyo, Japan) was dissolved at 4 mg/ml in 0.05 M acetic acid and then emulsified with an equal volume of complete Freund's adjuvant (Difco). For the primary immunization, 100 μl of the immunogen were injected intradermally into 8-week-old mice at the tail base. After 3 weeks, the mice received the same dose of immunogen subcutaneously. Arthritis developed within 10 days of the second immunization. These mice were kept under specific pathogen-free conditions in a clean room at the Animal Research Center, Institute of Medical Science, University of Tokyo.

Assessment of CIA disease severity. After physical examination, legs were scored as follows: 0, normal; 1, erythema and mild swelling confined to the ankle joint or toes; 2, erythema and mild swelling extending from the ankle to the midfoot; 3, erythema and severe swelling extending from ankle to the metatarsal joints; 4, ankylosing deformation with joint swelling[24]. The disease score for each mouse was calculated as the sum of the scores for the 2 hind legs.

Oral roxithromycin for CIA mice. RXM was dissolved in 5% arabic gum in 0.9% NaCl, and different doses of RXM (100, 200, 400, and 800 μg) were orally given to 5 different groups comprising 8 mice in each group. The 5% arabic gum, 0.9% NaCl combination alone was also given to the control mouse group orally. RXM or 5% arabic gum in 0.9% NaCl was given orally to mice every day up to Day 14 after second immunization of type II collagen.

ELISA of cytokines and type II collagen antibody levels in CIA mice. Serum samples from CIA mice were collected on the day of the first and second immunizations and Days 7, 14, and 21 after the second immunization. IL-6, TNF-α, IL-4, and IFN-γ levels were assayed by ELISA. Type II collagen antibody levels were assayed by ELISA (Chondrex, Redmond, WA, USA). Comparison of antibody levels was performed at 490 nm optical density.

Histology. Mice were euthanized by CO_2 asphyxiation and hind paws taken from CIA mice 3 weeks after the second immunization were fixed in 10% phosphate-buffered formalin (pH 7.4), decalcified in 10% EDTA, and embedded in paraffin. Sections (4 μm) were stained with hematoxylin and eosin.

Statistical analysis. Statistical analysis was performed by the 2-tailed Student's t test for all the assays (^{3}H-thymidine incorporation assay, ELISA, and transendothelial migration assay). Statistical differences of ankle width and paw width of CIA mice were assessed by Student t test, and the disease score was evaluated by Mann-Whitney U test.